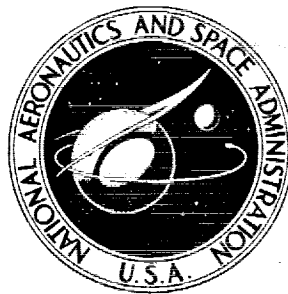


**NASA CONTRACTOR  
REPORT**



**NASA CR-2392**

**NASA CR-2392**

**EXPERIMENTS ON  
CONFINED TURBULENT JETS  
IN CROSS FLOW**

*by Yasuhiro Kamotani and Isaac Greber*

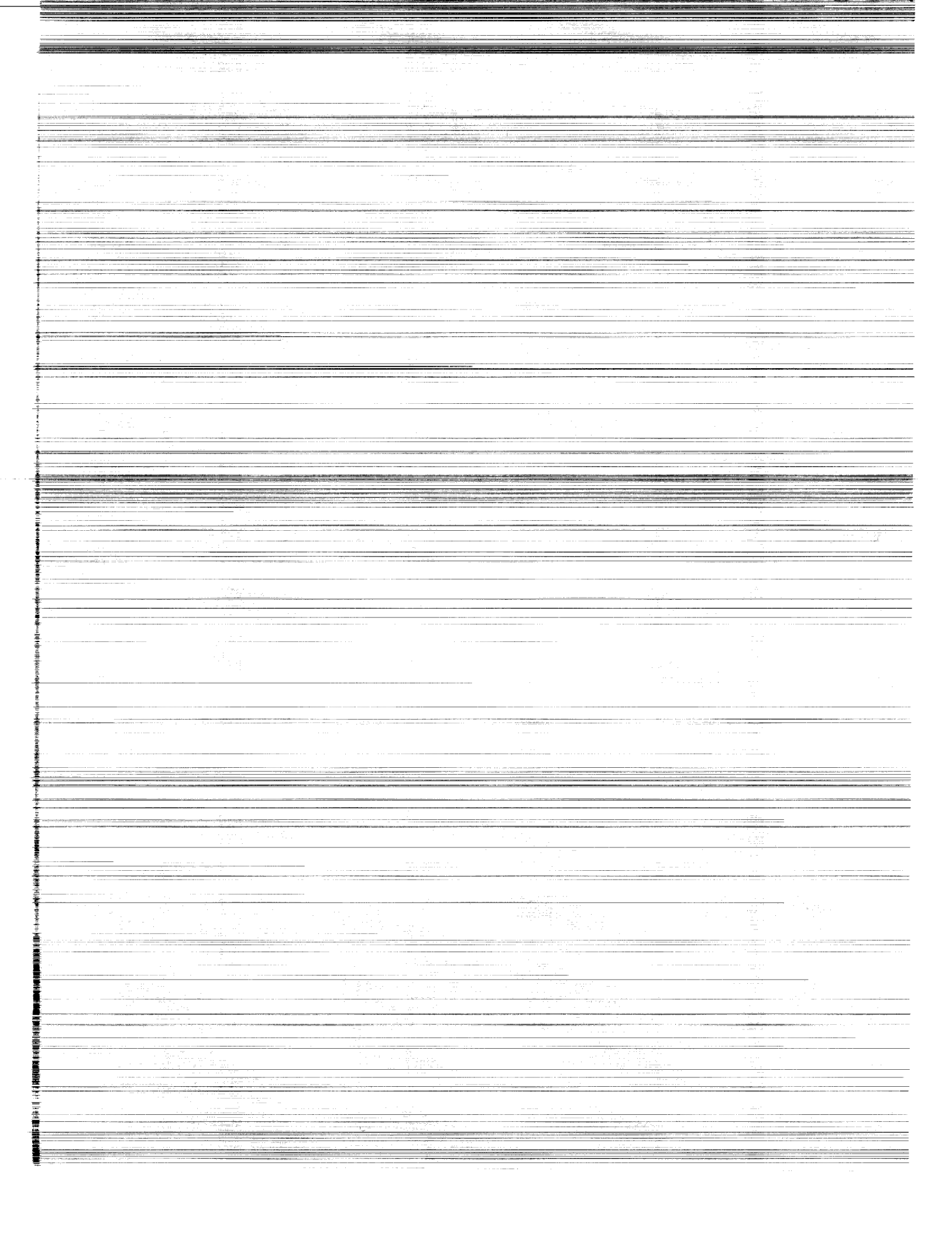
*Prepared by*

**CASE WESTERN RESERVE UNIVERSITY**

Cleveland, Ohio 44106

*for Lewis Research Center*

**NATIONAL AERONAUTICS AND SPACE ADMINISTRATION • WASHINGTON, D. C. • MARCH 1974**



1. Report No. <b>NASA CR-2392</b>	2. Government Accession No.	3. Recipient's Catalog No.	
4. Title and Subtitle <b>EXPERIMENTS ON CONFINED TURBULENT JETS IN CROSS FLOW</b>		5. Report Date <b>MARCH 1974</b>	6. Performing Organization Code
		8. Performing Organization Report No. <b>None</b>	10. Work Unit No.
7. Author(s) <b>Yasuhiro Kamotani and Isaac Greber</b>		11. Contract or Grant No. <b>NGL 36-027-008</b>	
9. Performing Organization Name and Address <b>Case Western Reserve University 2040 Adelbert Road Cleveland, Ohio 44106</b>		13. Type of Report and Period Covered <b>Contractor Report</b>	
		14. Sponsoring Agency Code	
12. Sponsoring Agency Name and Address <b>National Aeronautics and Space Administration Washington, D.C. 20546</b>		15. Supplementary Notes <b>Final Report. Project Manager, James D. Holdeman, Airbreathing Engines Division, NASA Lewis Research Center, Cleveland, Ohio</b>	
16. Abstract <b>Results are reported of experiments on the effects of an opposite wall on the characteristics of turbulent jets injected into a cross flow, for unheated and heated jets. Longitudinal and transverse distributions of velocity and temperature are presented for single and multiple circular jets, and trajectories are presented for two-dimensional jets. The opposite wall has relatively little effect on a single jet unless the ratio of jet to cross flow momentum flux is large enough for the jet to impinge on the opposite wall. For a row of jets aligned perpendicularly to the cross flow, the opposite wall exerts progressively larger influence as the spacing between jets decreases. Much of the effect of jet and wall proximity can be understood by considering the interaction of the vortex flow which is the major feature of the structure of a single jet in a cross flow. Smoke photographs are shown to elucidate some of the interaction patterns.</b>			
17. Key Words (Suggested by Author(s)) <b>Jet mixing; Jet penetration; Jets in crossflow; Combustion gas dilution</b>		18. Distribution Statement <b>Unclassified - unlimited</b>	
19. Security Classif. (of this report) <b>Unclassified</b>	20. Security Classif. (of this page) <b>Unclassified</b>	21. No. of Pages <b>75</b>	22. Price* <b>\$3.50</b>

\* For sale by the National Technical Information Service, Springfield, Virginia 22151



TABLE OF CONTENTS

	<u>Page</u>
I. INTRODUCTION	1
II. EXPERIMENTAL TECHNIQUE	3
III. RESULTS OF MEASUREMENTS	5
A. Confined Jet Experiments	5
(i) Jet Trajectories	5
(ii) Velocity and Temperature Distributions	10
B. Interaction of Multiple Jets	12
IV. CONCLUSIONS	15
REFERENCES	16
FIGURES	17

LIST OF FIGURES

	<u>Page</u>
Figure 1. Sketch of Experimental Setup	17
Figure 2. Velocity and Temperature Distributions at Jet Exit	18
Figure 3. Velocity Trajectories for Single Jet with Opposing Wall	19
Figure 4. Temperature Trajectories for Single Jet with Opposing Wall	20
Figure 5. Smoke Photographs of Single Jet with Opposing Wall	21
Figure 6. Velocity Trajectories for Two Opposing Jets	22
Figure 7. Velocity Trajectories for Two-dimensional Jet	23
Figure 8. Velocity Trajectories for Two-dimensional Jet	24
Figure 9. Correlation of Velocity Trajectories for Two-dimensional Jet with Opposing Wall	25
Figure 10. Comparison of Predicted Jet Trajectories for Two-dimensional Jet	26
Figure 11. Velocity Trajectories for Single Row of Jets	27
Figure 12. Velocity Trajectories for Single Row of Jets	28
Figure 13. Smoke Photographs of Single Row of Jets	29
Figure 14. Smoke Photographs of Single Row of Jets	30
Figure 15. Smoke Photographs of Single Row of Jets	31
Figure 16. Effect of Spacing Ratio on Jet Trajectories	32
Figure 17. Effect of Spacing Ratio on Jet Trajectories	33
Figure 18. Change of Jet Centerline Location with Spacing Ratio	34
Figure 19. Contours of Constant Speed and Temperature for Single Row of Jets	35

	<u>Page</u>
Figure 20. Contours of Constant Speed and Temperature for Single Row of Jets	36
Figure 21. Distribution of Velocity Vectors in the Plane of Symmetry for Single Row of Jets	37
Figure 22. Contours of Constant Speed and Temperature for Single Row of Jets	38
Figure 23. Contours of Constant Speed and Temperature for Single Row of Jets	39
Figure 24. Contours of Constant Speed and Temperature for Single Row of Jets	40
Figure 25. Contours of Constant Temperature for Single Jet	41
Figure 26. Contours of Constant Speed for Single Jet	42
Figure 27. Contours of Constant Speed for Two Opposing Jets	43
Figure 28. Temperature Distributions in the Plane of Symmetry for Single Row of Jets	44
Figure 29. Temperature Distributions in the Plane of Symmetry for Single Row of Jets	45
Figure 30. Temperature Distributions in the Plane of Symmetry for Single Row of Jets	46
Figure 31. Temperature Distributions in the Plane of Symmetry for Single Row of Jets	47
Figure 32. Temperature Distributions in the Plane of Symmetry for Single Row of Jets	48
Figure 33. Temperature Distributions in the Plane of Symmetry for Single Jet	49
Figure 34. Temperature Distributions in the Plane of Symmetry for Single Jet	50
Figure 35. Decay of Centerline Temperature for Single Row of Jets	51
Figure 36. Decay of Centerline Temperature for Single Row of Jets	52

	<u>Page</u>
Figure 37. Decay of Centerline Temperature for Single Row of Jets	53
Figure 38. Smoke Photographs of Multiple Jets	54
Figure 39. Velocity Trajectories for Multiple Jets	55
Figure 40. Comparison of Jet Trajectories	56
Figure 41. Contours of Constant Speed and Temperature for Multiple Jets	57
Figure 42. Contours of Constant Speed for Multiple Jets	58
Figure 43. Smoke Photographs of Multiple Jets	59
Figure 44. Contours of Constant Speed and Temperature for Multiple Jets	60
Figure 45. Contours of Constant Speed and Temperature for Multiple Jets	61
Figure 46. Contours of Constant Speed at Several Downstream Locations	62
Figure 47. Contours of Constant Speed and Temperature for Multiple Jets	63
Figure 48. Contours of Constant Speed and Temperature for Multiple Jets	64
Figure 49. Smoke Photographs of Multiple Jets	65
Figure 50. Contours of Constant Speed and Temperature for Multiple Jets	66
Figure 51. Contours of Constant Speed and Temperature for Multiple Jets	67
Figure 52. Smoke Photographs of Multiple Jets	68
Figure 53. Contours of Constant Speed and Temperature for Multiple Jets	69

## SYMBOLS

- $A_j$  jet cross sectional area  
 $B$  constant in trajectory equation (1)  
 $D$  diameter of round nozzle or width of two-dimensional nozzle  
 $D_1$  effective diameter of a pair of nozzles; see Fig. 37  
 $H$  distance from nozzle to opposite wall; see Fig. 1

$J$  jet to cross flow momentum ratio;

$$J = \frac{1}{\rho_o U_o^2 A_j} \int \rho_j U_j^2 dA_j$$

- $S$  distance between centers of nozzles  
 $\bar{T}$  time average temperature  
 $T_o$  cross flow temperature  
 $T_j$  initial jet temperature  
 $\bar{U}$  time average velocity  
 $U_o$  cross flow velocity  
 $U_j$  initial jet velocity  
 $u$  non-dimensional velocity,  $\bar{U}/U_o$   
 $x$  downstream distance from nozzle center; see Fig. 1  
 $Y$  distance from nozzle perpendicular to  $X$  and  $Z$ ; see Fig. 1  
 $Z$  vertical height above nozzle; see Fig. 1  
 $Z_T$  vertical height of temperature trajectory  
 $Z_v$  vertical height of velocity trajectory

$\theta$  temperature parameter;

$$\theta = \frac{\bar{T} - T_o}{T_j - T_o}$$

- $\rho_o$  cross flow density  
 $\rho_j$  initial jet density



## I. INTRODUCTION

In previous papers<sup>1,2</sup> results of experiments on a single jet issuing perpendicularly into an unbounded cross stream were reported. The work was a first step in the study of the mixing of combustion gases with cooling air in gas turbine combustors. It was found that (1) the velocity distributions depend mainly on the ratio of jet to cross flow momentum flux; (2) the temperature distributions and the jet structure also depend weakly on the jet to cross flow density ratio; (3) a pair of vortices forms behind the jet, and the vortex structure becomes the dominant feature of the jet in the far downstream region; (4) the entrainment rates are nearly independently controlled by the components of cross flow normal and parallel to the jet trajectory.

The work has been continued to examine basic jet interaction patterns similar to those which occur in combustor configurations. In the present paper results are reported of experiments on (1) a single round jet, a single row of equally spaced round jets, or a two-dimensional jet injected perpendicularly into a confined air passage; (2) interaction patterns of two or three round jets in an unbounded cross stream. Velocity distributions were measured with jets and cross flow at the same temperature. As in the previous experiments on a single jet, cross flow temperature dilution was studied by making the temperature of the jets higher than that of the cross flow because of experimental simplicity. The results of the unheated and heated jet experiments are expected to be applied deductively to the cooling problem. The results also have

application to other problems such as the structure of plumes from chimneys, V/STOL aircraft using air jets to obtain lift for takeoff, etc.

## II. EXPERIMENTAL TECHNIQUE

Experiments were conducted in a 71 cm. square cross section subsonic wind tunnel. Air velocities at the test section ranged from about 6 to 9 m/sec. Fig. 1 illustrates the basic experimental setup, and defines most of the symbols used herein. The height of the wall (H) was adjustable. In measurements of a single row of jets or a two-dimensional jet the total width of the jet configuration was much less than the 71 cm. width of the tunnel, so side walls within the tunnel were used. Bottom, top, and side walls were made of .635 cm. thick plexiglas plate. In most of the experiments jets were injected from straight steel pipes of .635 cm. I.D. and about 18 cm. long. In some of the single jet experiments the jet was injected from a carefully shaped nozzle with .635 cm. dia. exit, which gave low turbulence (turbulence level 0.3%) and nearly flat velocity and temperature distributions at the exit. Velocity profiles at the pipe exits correspond to that of fully developed turbulent flow, with a turbulence level at the center of 2.4%. Representative velocity and temperature profile of a nozzle and a pipe are shown in Fig. 2. It was found that the trajectory of a jet from a pipe can differ by about 10% from the trajectory from a nozzle, but the structure of the two jets was very similar. To minimize the effect of the tunnel wall boundary layer the exit planes of both the pipes and the nozzle were set flush with a flat plate placed 7.6 cm. above the bottom wall of the wind tunnel.

Experiments were performed over a range of momentum ratios  $J$  of 8 to 72. Multiple jet experiments were performed for spacing ratios  $S/D$

ranging from 2 to 12, plus the single jet experiments, which is essentially the limit as the spacing ratio becomes very large. In the two-dimensional jet experiments the jet was injected from a slit .635 cm. wide and 15 cm. long, spanning the distance between side walls.

Velocity was measured in unheated jets using a hot wire probe operated by a Shapiro and Edwards Model 50 constant current hot wire anemometer. For heated jet experiments air was heated up to  $167^{\circ}$  K ( $300^{\circ}$  F) above cross flow temperature, using a Chromalox Circulation Heater with a sensitive temperature control unit. Temperature was measured using iron-constantan thermocouples.

### III. RESULTS OF MEASUREMENTS

#### A. Confined Jet Experiments

(i) Jet Trajectories. The same definitions of jet trajectories for a single jet are used here as were used and whose rationale was discussed in Refs. 1 and 2. The velocity trajectory is the locus of the maximum velocity in the plane of symmetry, and the temperature trajectory is the locus of the maximum temperature in the plane of symmetry. Jet velocity trajectories with and without an opposite wall are shown in Fig. 3 for several momentum ratios and wall spacings. It is seen that the trajectory is not very sensitive to the opposite wall location unless the jet approaches the wall quite closely. The cross flow passes around the jet, and does not exert much pressure force on it. Correspondingly, the temperature trajectories are also insensitive to opposite wall location, as is seen in Fig. 4.

If  $J$  is sufficiently large for a given  $H/D$ , the jet directly impinges on the wall and a region of upstream-moving flow occurs. Fig. 5 shows some smoke photographs of the single jet with an opposite wall. The impingement on the opposite wall at the higher momentum ratios is quite evident. Even including these impingement cases, the jet velocity trajectory, as defined above, remains closely approximately by the equation given by Kamotani and Greber<sup>1</sup> for an unbounded single jet; that is

$$\frac{z}{D} = BJ^{0.47} \left(\frac{x}{D}\right)^{0.36} \quad (1)$$

where the constant  $B$  is 0.89 for a jet from a nozzle (flat initial profile) and 0.81 for a jet from a pipe (fully developed initial profile).

Since the jet keeps rising and spreading, it eventually approaches the upper wall, and the trajectory starts deviating from the correlation expressed in Eqn. (1).

A few experiments were conducted in which two jets impinged on each other, in order to compare the behavior with that of interaction with an opposite wall. Fig. 6 shows velocity trajectories for several momentum ratios and one wall spacing ratio for both opposite jet impingement and an opposite wall. One sees that the trajectories are virtually indistinguishable from each other. As far as the velocity trajectories are concerned the plane of symmetry between two opposing jets can be considered equivalent to a wall. However, for this to be true it is very important that the velocities of the two opposing jets be matched very closely.

The opposite extreme from the single jet configuration is a two-dimensional jet, in these experiments generated by injecting a jet through a slit spanning the air passage. In contrast to the single round jet case, the trajectory of the two-dimensional jet depends very strongly on the upper wall location. Some representative trajectories of the two-dimensional jet for several momentum ratios and wall locations are shown in Figs. 7 and 8. One sees that with a distant opposing wall the two dimensional jet has a higher trajectory than a round jet, but is lowered sharply as the upper wall is lowered. It is rather easy to see that, without lowering the trajectory, decreasing the gap between the walls would be associated with large pressure differences across the jet, since the cross flow cannot pass around the two-dimensional jet

as it does past the round jet. A correlation of the two-dimensional jet trajectories is shown in Fig. 9. For  $Z < H/2$  the trajectory can be expressed as:

$$\frac{Z}{D} = 2.0J^{0.28} \left( \frac{x}{D} \right)^{0.5} (1 - e^{-0.07 \frac{H}{D}}) \quad (2)$$

The trajectory is a parabola for all wall spacings, and the factor giving the height variation with wall spacing is independent of the momentum ratio. Fig. 10 presents a comparison of the present trajectory correlation for two-dimensional unbounded jets. Vizel and Mostinskii<sup>3</sup> calculate the trajectory by assuming that the jet experiences a cross force which is proportional to the cross flow dynamic pressure. The constant of proportionality is obtained by fitting the result to the trajectory data of Ivanov<sup>4</sup>. The assumption of a constant cross force leads directly to a parabolic trajectory, in agreement with the present data. The magnitudes and dependence on momentum ratio differ from the present results. Abramovitch<sup>5</sup> estimates the trajectory by assuming that the local velocity at the centerline is the sum of the cross flow velocity and a component whose magnitude is the free jet similarity value and whose direction is the local direction of the curved jet. This is seen to yield higher jet trajectories and different trajectory shapes from the Vizel and Mostinskii or the present results.

With the results for the single round jet and the two-dimensional jet, one can more readily examine the more practical configuration of a row of equally spaced round jets. Figs. 11 and 12 show representative

trajectories of the middle jet in a single row, for various momentum ratios  $J$ , wall spacing ratios  $H/D$ , and jet spacing ratios  $S/D$ . Each figure shows trajectories for three momentum ratios: a low, a high, and an intermediate value. The curves for intermediate momentum ratio, which fall between those for low and high momentum ratio, are plotted separately to keep the graphs readable. Sample smoke photographs are shown in Figs. 13, 14, 15. Examining the close spacing  $S/D = 2$  (Figs. 11 and 13), the smoke photographs indicate a combined jet looking very much like a two-dimensional jet. The trajectory measurements show that the trajectory is noticeably suppressed as  $H/D$  decreases, and that the amount of suppression depends on  $J$ . One expects this, since each jet spreads faster as  $J$  increases, and the combined jet behaves more like a two-dimensional jet. For a moderate spacing,  $S/D = 4$  (Figs. 12 and 14), one sees from the measurements that the effect of the upper wall on the trajectory becomes small even for high values of  $J$ . The reason for this appears in the photographs, which show that there is an upstream region in which the individual jets are distinct, and behave more independently than at closer spacing. For still higher spacing ratio,  $S/D = 6$  (Fig. 15), the photographs show that the jets remain separate from each other for quite some distance downstream; correspondingly the effect of the opposite wall on the trajectory becomes small.

Figures 16 and 17 present trajectories for two momentum ratios and several jet spacings, for opposite walls sufficiently far from the nozzles so that the suppression effect of the opposite wall is negligible. Note that to achieve negligible suppression, the wall spacing must be

larger for the two dimensional jet than is required for a row of spaced jets. The figures serve to emphasize the role of jet interaction on the trajectories. Starting with the single jet trajectory, one sees that as the jet spacing becomes smaller and the jets start interacting the trajectory is lowered. However, for sufficiently close spacing the trajectory rises eventually approaching the very high two-dimensional trajectory. For wide spacing the trajectory shapes are similar to those of a single jet; for close spacing they approach the shape of a two-dimensional jet. Fig. 18 shows the variation of the trajectory height with spacing ratio, at a given non-dimensional downstream location, for several momentum ratios. It illustrates the manner in which the trajectory is first suppressed from the single jet value, then rises to the two-dimensional value, as spacing ratio decreases.

The above behavior can be accounted for by considering the vortex structure of well separated jets, and the effect of closeness on the vortex interaction and the entrainment process. Representing the jet in cross-section as a pair of counter-rotating vortices, one sees that two pairs of vortices will drive each other downward, and hence the trajectories of a row of jets will become lower as the spacing decreases. This model alone would predict continually lowered trajectories with decreasing spacing. For sufficiently close spacing, however, the initial vortices are relatively weak (they vanish in the two-dimensional jet limit), and the jets interfere with each others entrainment of cross flow. This latter effect results in slower decay of the initial upward momentum flux of the jet. Consequently for close enough spacing the

jets maintain upward momentum longer, and experience only limited deflection due to mutual vortex interaction.

(ii) Velocity and Temperature Distributions. Velocity and temperature distributions in planes perpendicular to the cross flow were measured. In the downstream region these are almost planes perpendicular to the trajectory directions. Some typical contours of constant speed and constant temperature are shown in Figs. 19 and 20 for a close spacing,  $S/D = 2$ , for two momentum ratios  $J = 8$  and  $72$ , and one wall spacing ratio,  $H/D = 24$ . Sufficiently close to the nozzles the trace of each jet is clearly visible, in the temperature contours for  $J = 72$  and in both the velocity and temperature contours for  $J = 8$ . However, at this close spacing ratio the jets mix quickly, and at relatively short distances downstream evidence of the individual jets disappears. One sees in Figs. 19 and 20 that at the short downstream locations only a weak periodic structure is left of the original jets. One finds no trace of vortex activity, even at the upstream locations, because only a small amount of cross flow passes through the space between the jets. Downstream of the jet openings a standing eddy is formed. This is seen in Fig. 21, which presents a sample set of velocity vectors in the plane of symmetry of the middle jet. The velocity in the eddy is very small, but highly turbulent. The standing eddy was observed for all momentum ratios investigated, but it disappears as the spacing increases. No eddy was observed for  $S/D \geq 4$ .

Fig. 22, 23, 24 show velocity and temperature contours for larger spacing,  $S/D = 4$  and  $6$ . Here at upstream locations the velocity contours

display the typical kidney shape of a single jet with vortex motion. As  $S/D$  increases, the vortex motion becomes stronger and the structure of each jet approaches that of a single jet in an unbounded stream.

When  $H/D$  is sufficiently small, a single jet impinges on the upper wall, the jet spreads sidewise along the wall, and momentum and temperature are carried away with the fluid in vortex motion. The result is that the jet is split into two parts, one on either side of the midplane. Half of this structure, showing the bifurcation, is seen in the speed and temperature contours of Figs. 25 and 26.

Fig. 27 shows velocity distributions for two opposing jets and for a jet with an opposite wall for the same momentum ratio and stream-wise location. The plane of symmetry of the jet pair is in the same location as the wall of the jet with an opposite wall. One sees that the distributions are almost identical, as was previously found for the trajectory. Farther downstream, of course, the distributions must be somewhat different because the velocity must be zero at the wall whereas it can become non-zero at the plane of symmetry.

Figures 28-32 show temperature contours in the plane of symmetry, for several spacing ratios and momentum ratios. At close spacing,  $S/D = 2$  (Figs. 28 and 29), one sees evidence of the standing eddy previously evident in the velocity vectors shown in Fig. 21, and the strong suppression effect of an upper wall. At larger spacing ratio,  $S/D = 4$  and 6 (Figs. 30-32), the temperature profiles no longer give evidence of eddy formation. Figs. 33 and 34 shows the corresponding temperature contours for a single jet. The single jet contours show no eddy formation, and again emphasize

that the suppression effect of an upper wall is small in this case.

Figs. 35-37 show the decay of maximum temperature in the plane of symmetry. Figs. 35 and 36 display together curves for a single momentum ratio and several spacing ratios. For  $S/D$  of 4 and larger, in the upstream region the decay is similar to that of a single jet, as is seen in the figures. In the downstream region the jets mix, and the decay approaches that of the two dimensional jet. For  $S/D$  of 2, mixing occurs very quickly, and there is no region in which the behavior is like a single jet. In addition, for  $S/D = 2$  the jet attaches to the wall and forms a standing eddy, as was previously discussed. In the present insulated wall measurements, the maximum temperature is then found to occur at the wall in the downstream region. Fig. 37 displays together curves for a single spacing ratio and several momentum ratios. One sees that the variation with momentum ratio is relatively weak, and becomes less important as spacing ratio decreases; for  $S/D = 2$  the decay is virtually independent of momentum ratio.

#### B. Interaction of Multiple Jets

To investigate certain detail features of jet interaction occurring in single and multiple row jets, two or three jets were placed in a cross flow wall. When two closely spaced jets are arranged parallel to the cross flow, the rear jet is in the wake of the front one, where the cross flow speed is very small. Consequently the rear jet is almost undeflected until it meets the front jet, and the two jets are quickly combined. This is seen in the smoke photographs in Fig. 38. Sample trajectories are shown in Fig. 39, and compared with

the single jet trajectory in Fig. 40. It is seen that the trajectory of the combined jet is slightly higher than that of a single jet injected from a nozzle having the same cross-sectional area as the sum of the two individual jets. Figs. 41 and 42 show sample velocity and temperature distributions, which are qualitatively similar to those of a single jet.

When two jets are placed side by side normal to the cross flow, the jet structure changes noticeably with the spacing ratio and the momentum ratio, as previously seen in the results for a row of jets. Fig. 43 shows smoke photographs and Figs. 44-46 show velocity and temperature contours for this configuration. The velocity contours show that there is no vortex activity between the two jets. The temperature contours display peaks at the "centers" of the two jets. Both the contours and the dark line in the photograph separating the two jets give evidence of the incomplete mixing of the jets. For three or more jets arranged in this way, the jet structure is very much like that for a long row except at the edges, where the structure is similar to the two jet structure. Velocity and temperature contours indicating this behavior are shown in Figs. 47 and 48.

Sample contours and smoke photographs for three equal jets, whose nozzle centers lie at the vertices of an equilateral triangle, are shown in Figs. 49-53. One sees both from the contours and photographs that the sidewise spreading and the degree of separation of the jets is significantly less if the single jet is upstream (Figs. 49-51) than if the single jet is downstream (Figs. 52 and 53). The qualitative structure

of the triangular configuration is insensitive to spacing ratio for  $S/D$  between 2 and 6, and to momentum ratio for  $J$  between 8 and 72. One expects that the qualitative structures of a double row of jets can be closely inferred from the single row and equilateral triangle results.

#### IV. CONCLUSIONS

1. Trajectories and structure of a single jet in a cross flow are only mildly affected by an opposite wall, unless the momentum ratio is sufficiently strong so that the jet directly impinges on the wall.
2. The trajectories and structure of a single row of jets depends strongly on the momentum ratio and the spacing ratio. For close spacing the behavior approaches that of a two-dimensional jet, and for wide spacing approaches that of a single jet. Trajectories are most suppressed for some intermediate value of spacing ratio, depending upon momentum ratio.
3. Temperature decay of a single row of jets, for moderate spacing, is similar to that of a single jet in an upstream region, and approaches that of a two-dimensional jet in the well mixed downstream region.
4. For two opposing jets, the plane of symmetry can be regarded as equivalent to an opposite wall in determining velocity trajectories and distributions in regions away from impingement with the wall.

## REFERENCES

1. Kamotani, Y. and Greber, I. : "Experiments on a Turbulent Jet in a Cross Flow," AIAA Journal, Vol. 10, No. 11, November 1972, pp. 1425-1429.
2. Kamotani, Y. and Greber, I. "Experiments on a Turbulent Jet in a Cross Flow," Report FTAS/TR-71-62 (NASA CR-72893), Div. of Fluid, Thermal and Aerospace Sciences, Case Western Reserve U., June 1971.
3. Vizel, Y.M. and Mostinskii, I.L. "Deflection of a Jet Injected into a Stream," Journal of Engineering Physics, Vol. 8, No. 2, 1965.
4. Ivanov, Y.V. : "Efficient Combustion of Super-Strate Fuel Gases in Furnaces," Estrosizdat, Tallin, 1959, also quoted in Ref. 3.
5. Abramovich, G.N. : The Theory of Turbulent Jets, M.I.T. Press, 1963.

Wind Tunnel Test Section  
71 cm X 71 cm

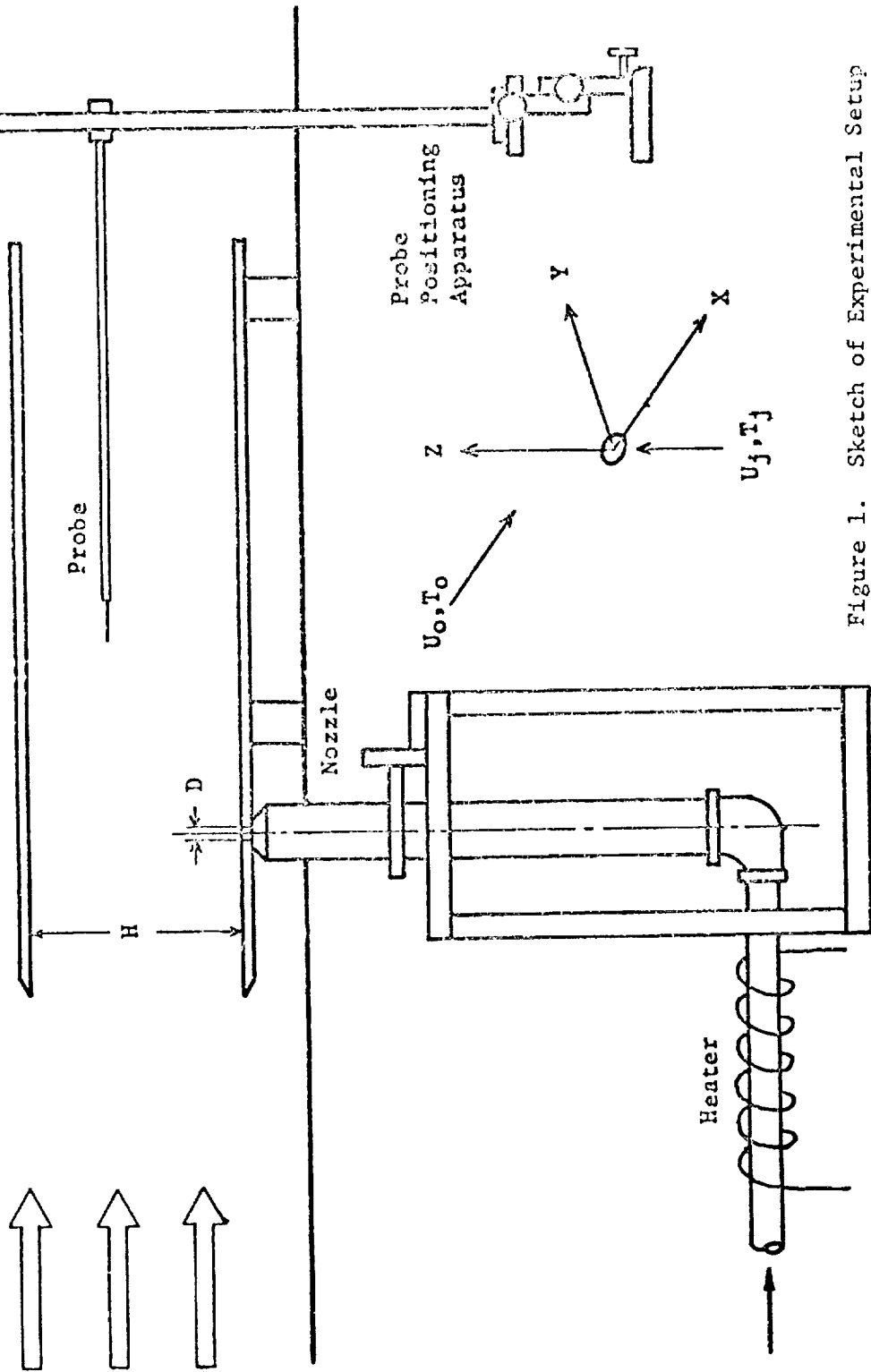


Figure 1. Sketch of Experimental Setup

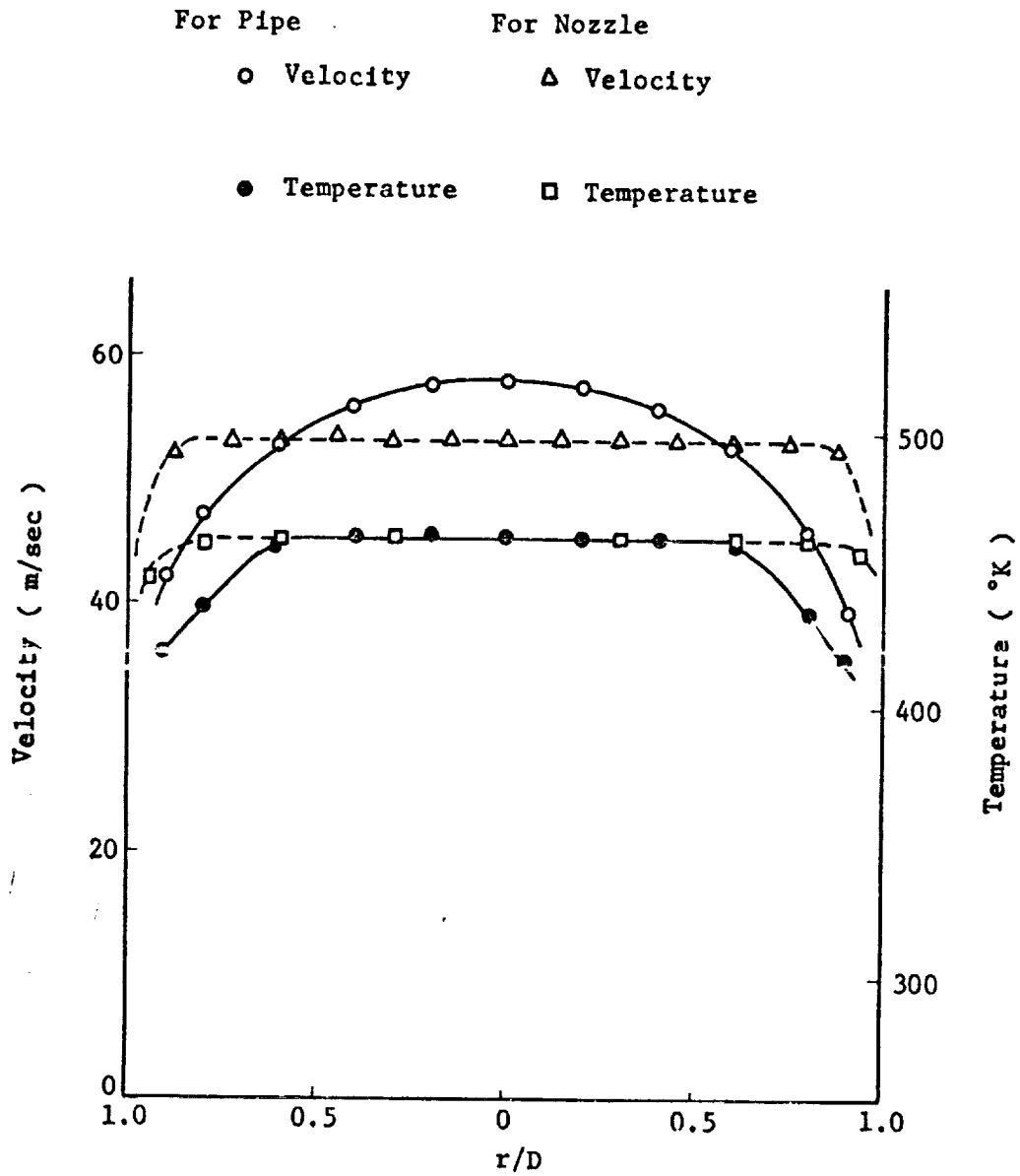


Figure 2. Velocity and Temperature Distribution at Jet Exit

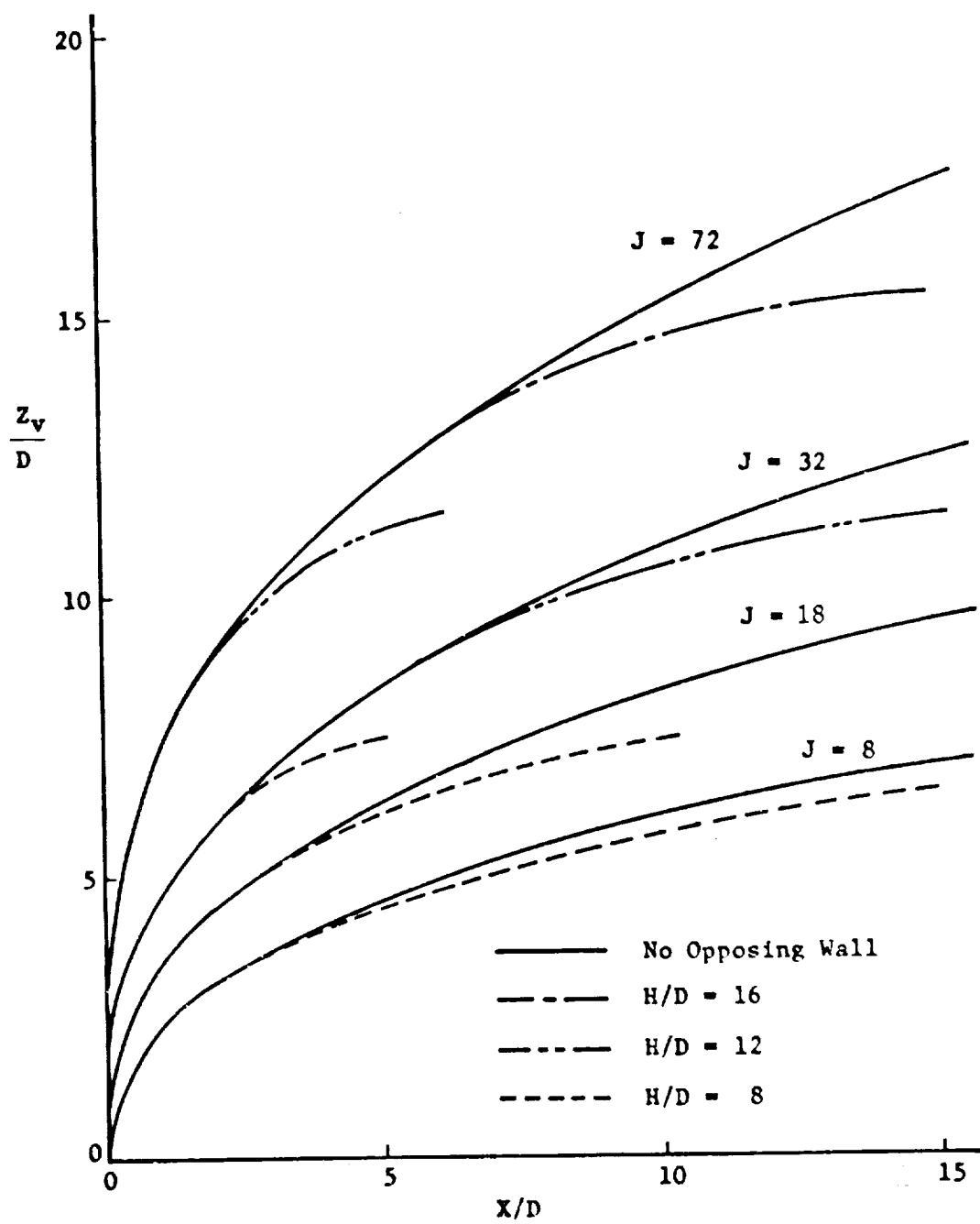


Figure 3. Velocity Trajectories for Single Jet with Opposing Wall

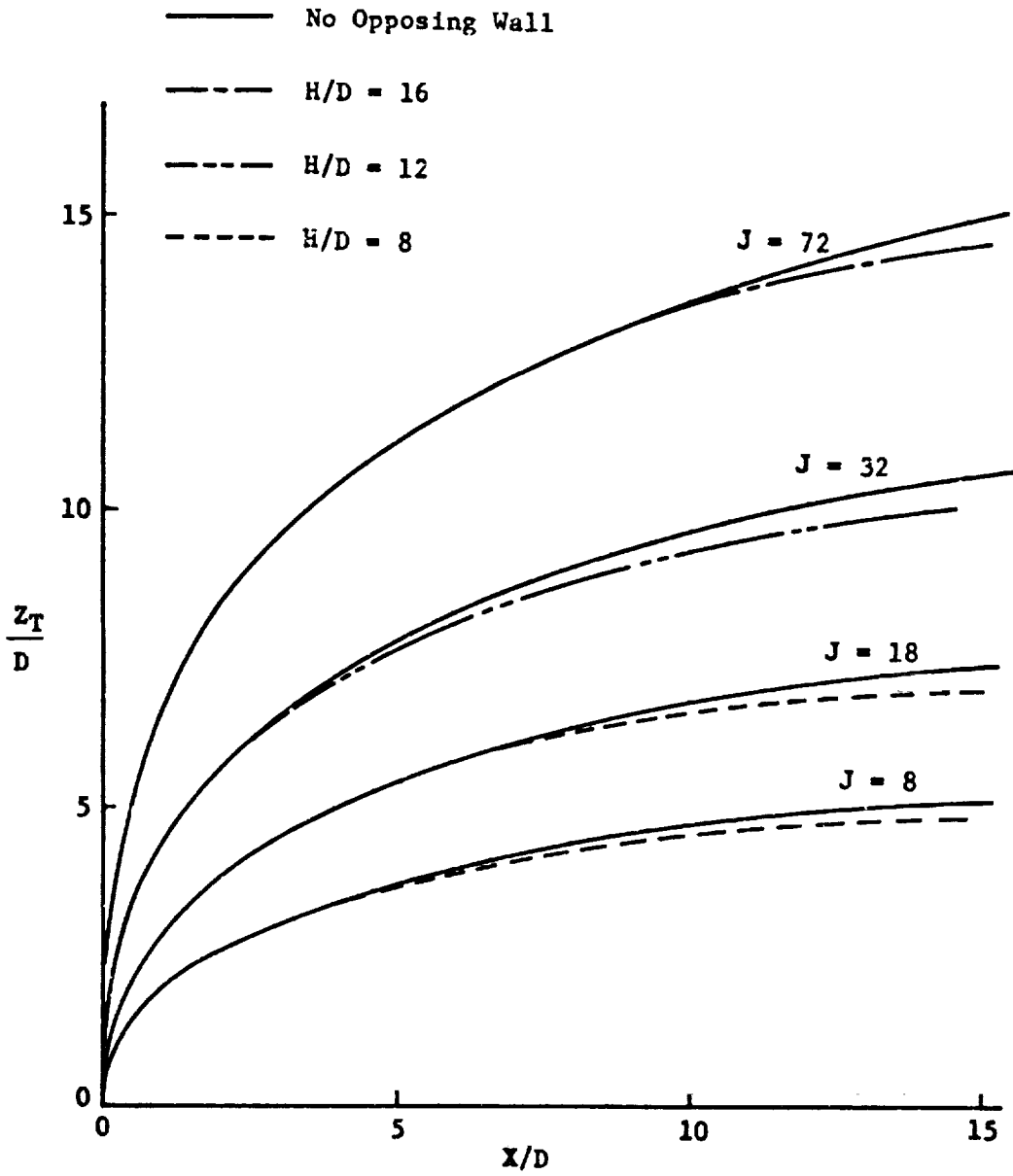
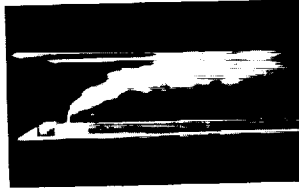


Figure 4. Temperature Trajectories for Single Jet with Opposing Wall

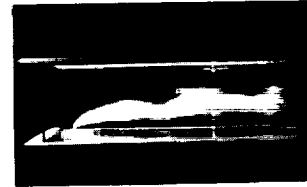
H/D = 16



J = 72



J = 18



J = 8

H/D = 12



J = 72

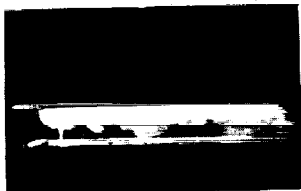


J = 18



J = 8

H/D = 8



J = 72



J = 18



J = 8

Figure 5. Smoke Photographs of Single Jet with Opposing Wall

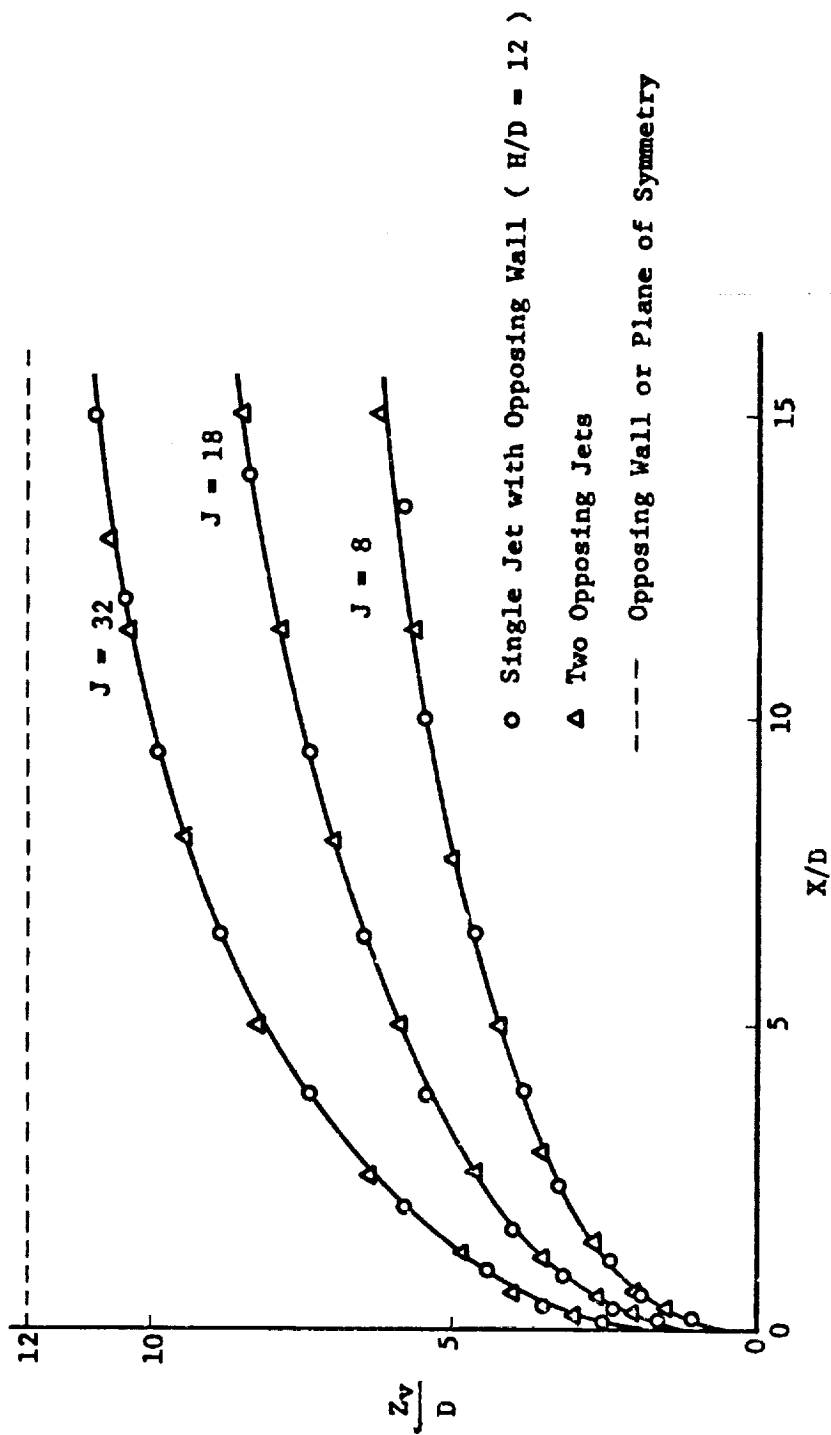


Figure 6. Velocity Trajectories for Two Opposing Jets

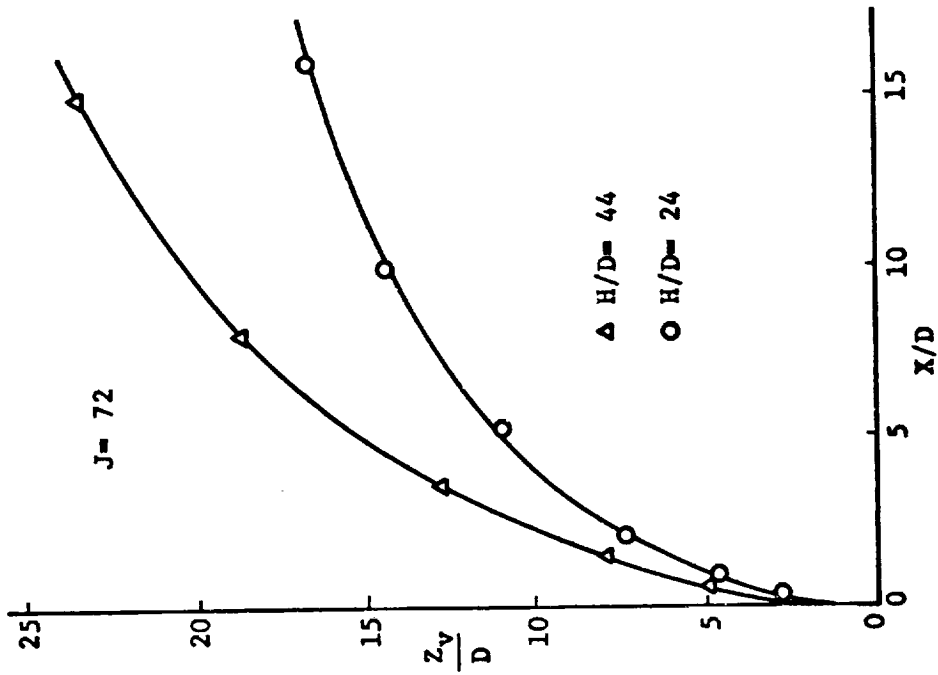
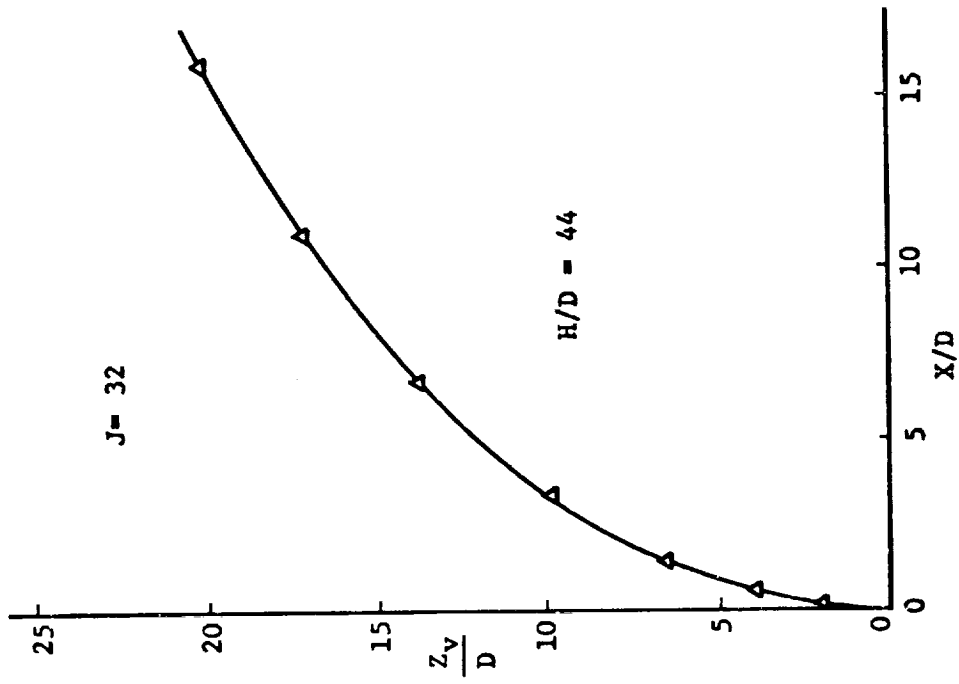


Figure 7. Velocity Trajectories for Two-dimensional Jet

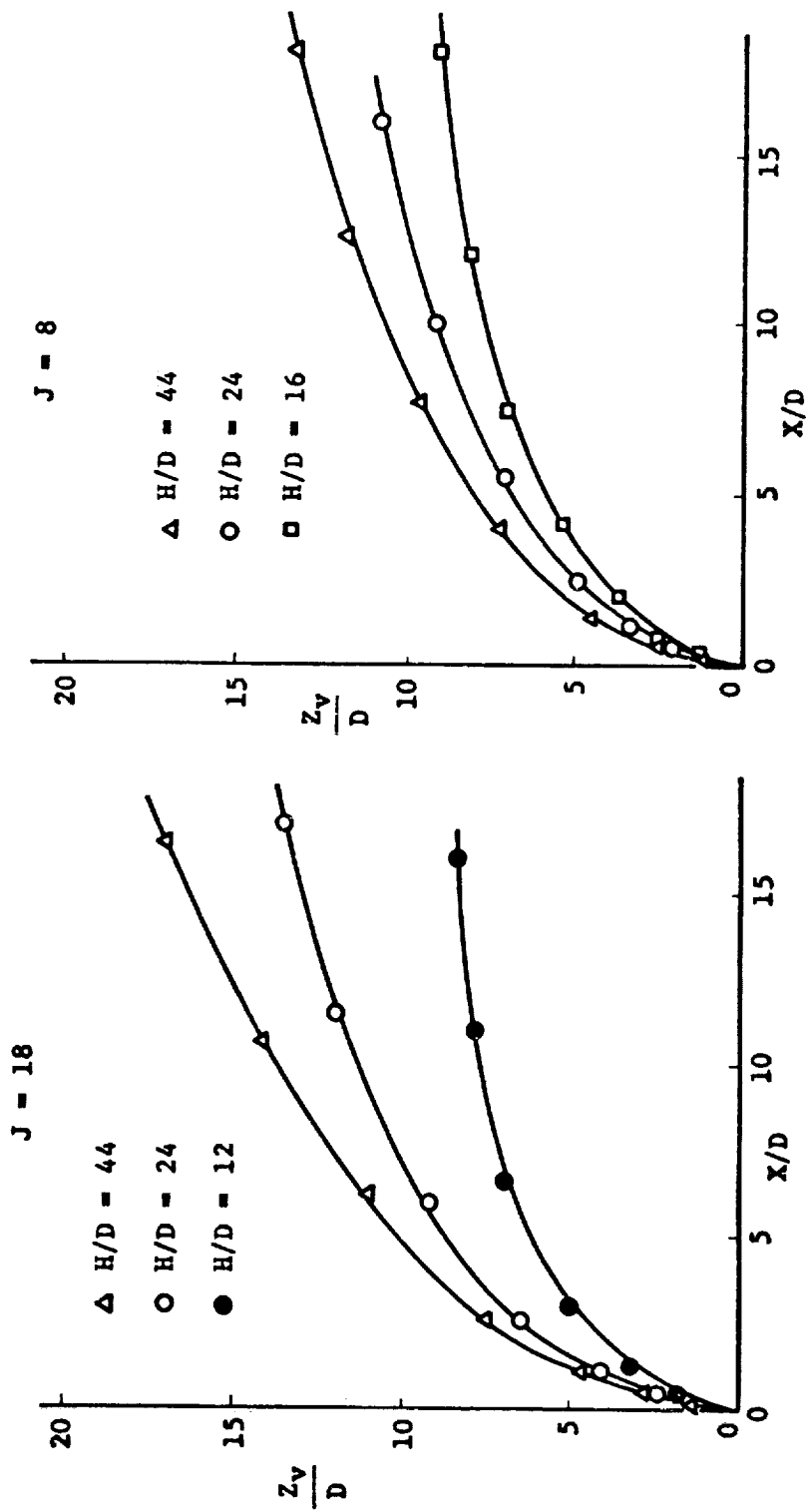


Figure 8. Velocity Trajectories for Two-dimensional Jet

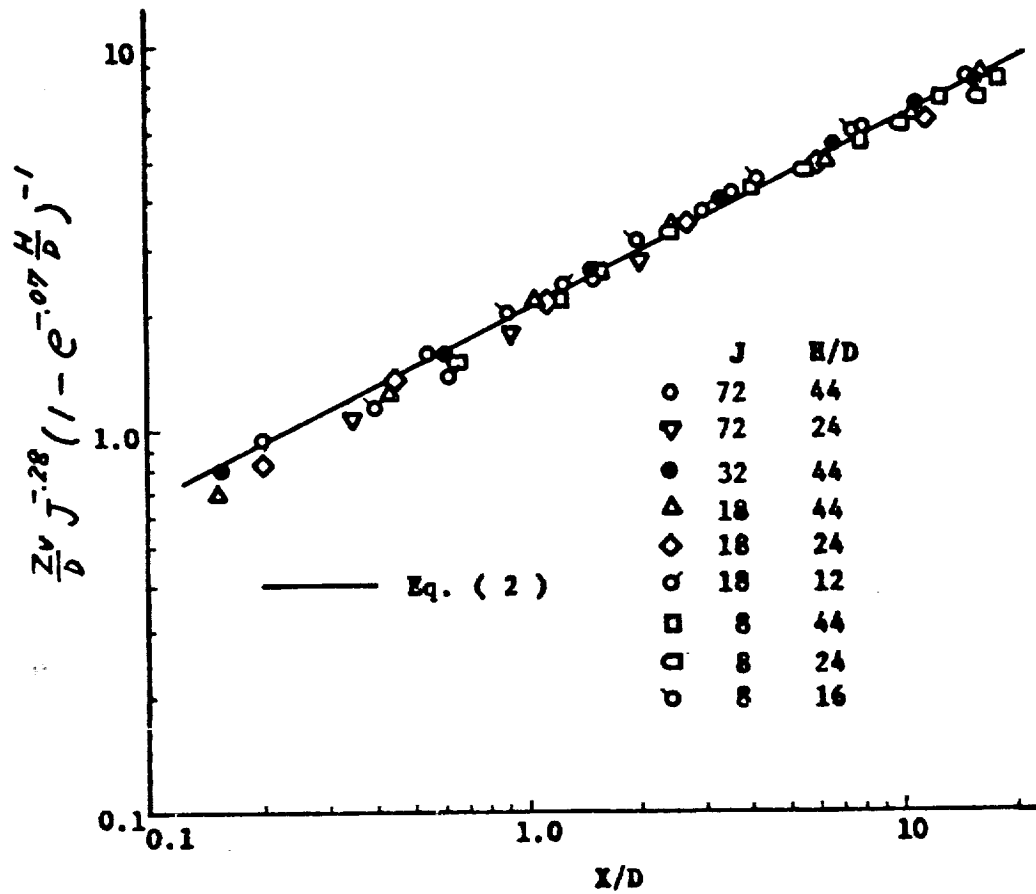


Figure 9. Correlation of Velocity Trajectories for Two-dimensional Jet with Opposing Wall

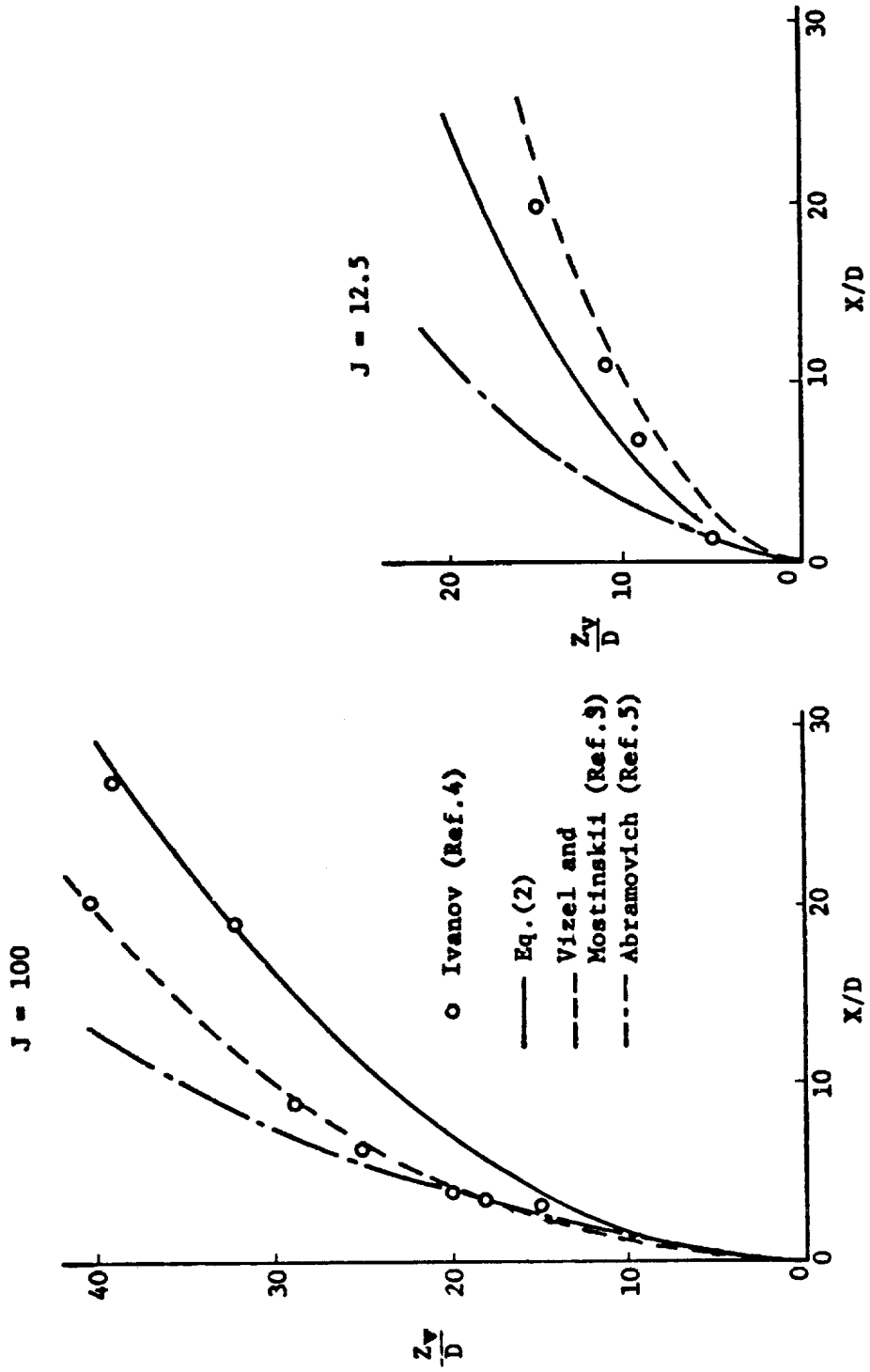


Figure 10. Comparison of Predicted Jet Trajectories for Two-dimensional Jet

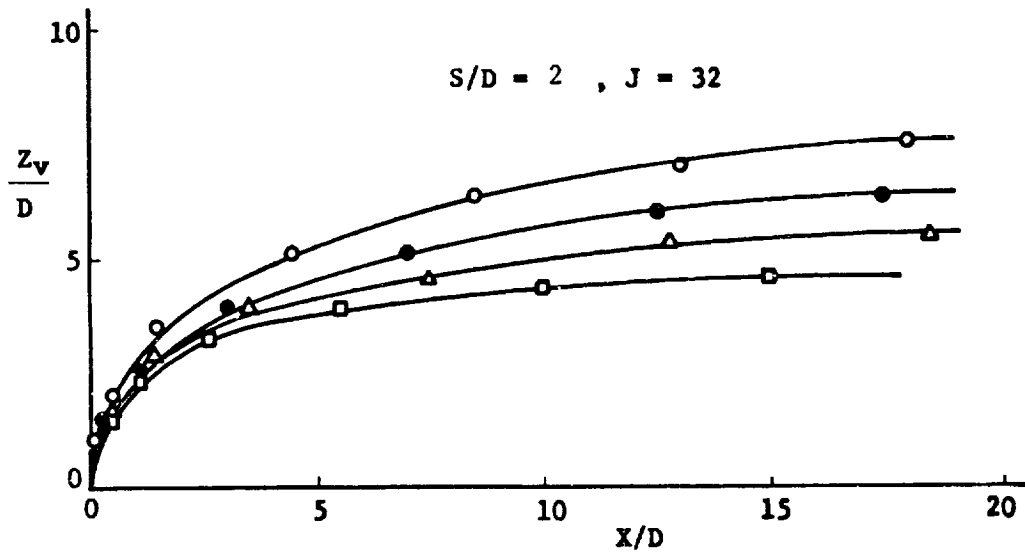
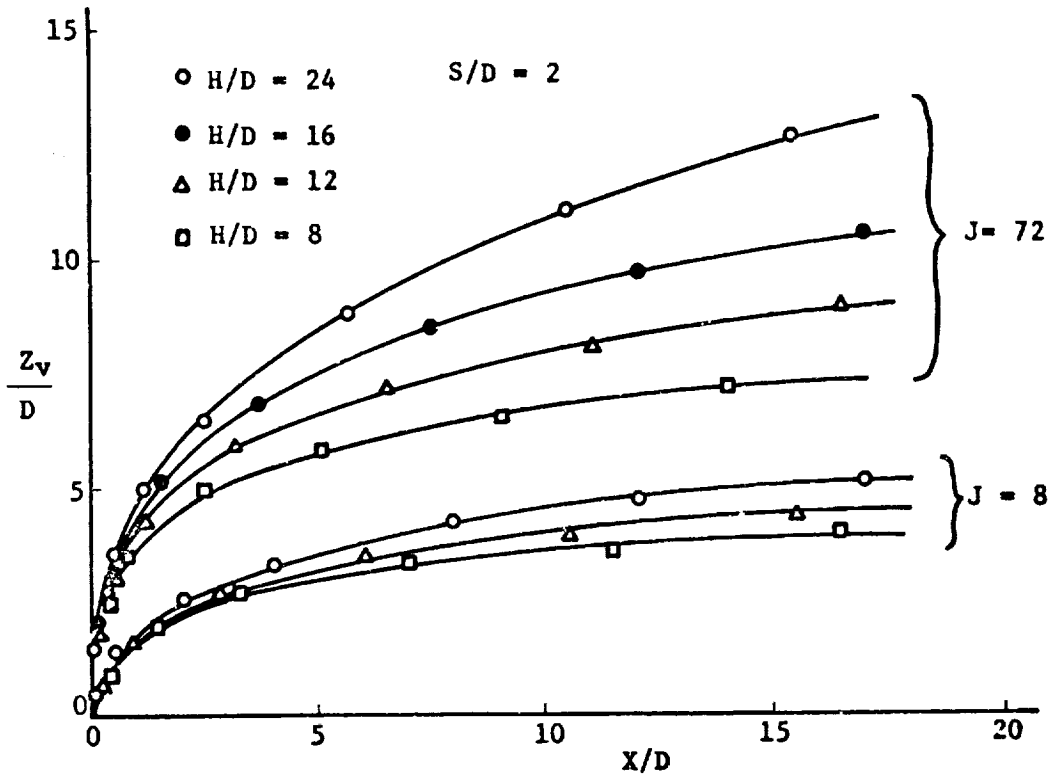


Figure 11. Velocity Trajectories for Single Row of Jets

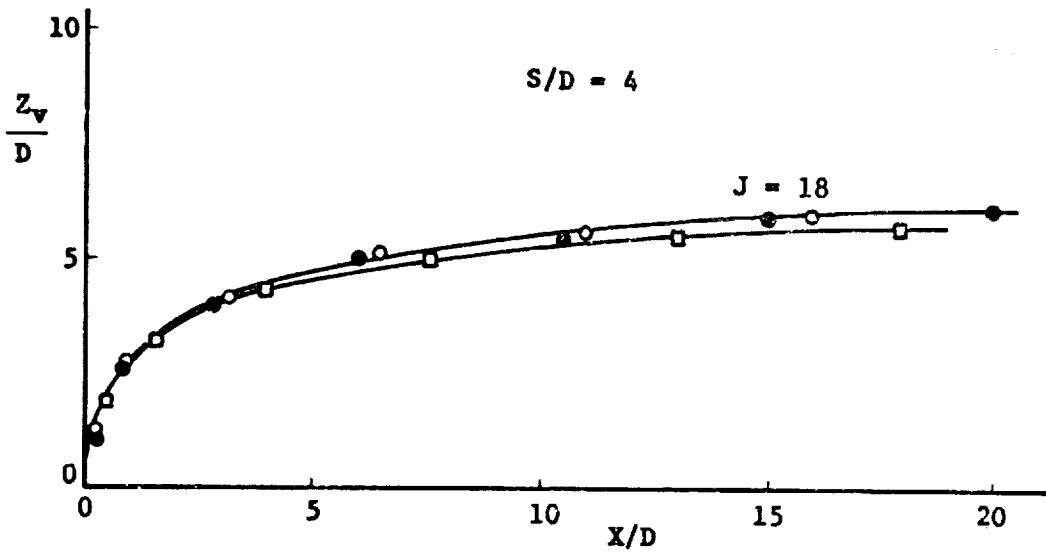
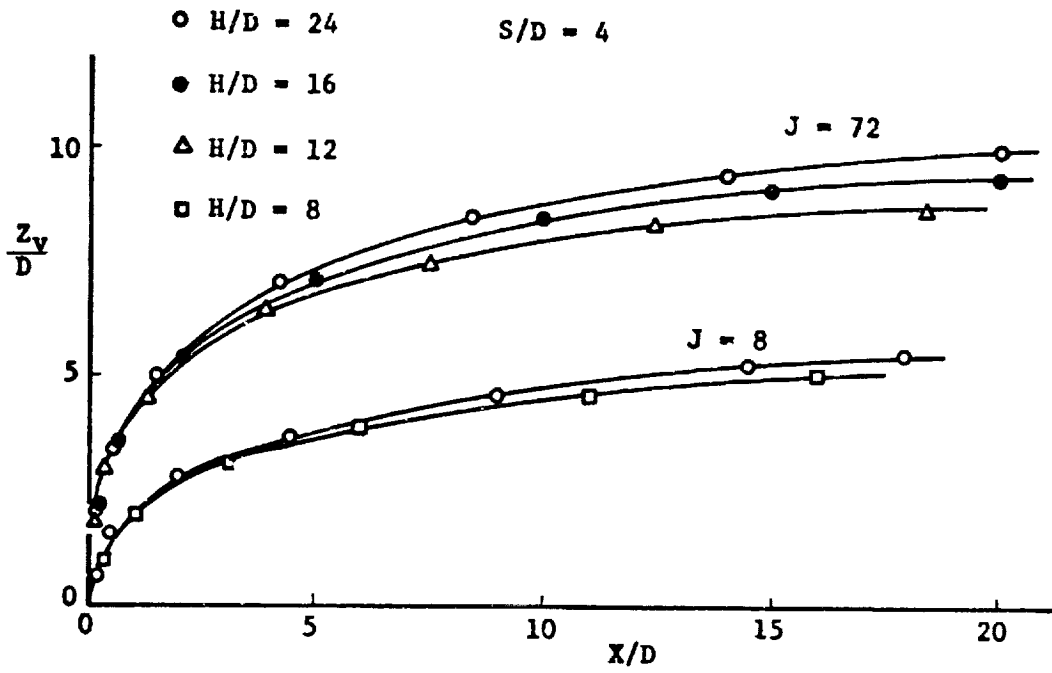
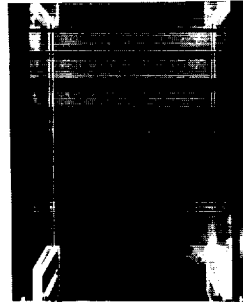
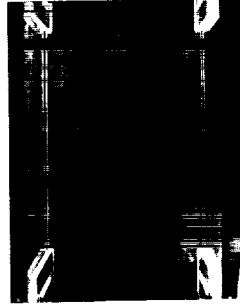
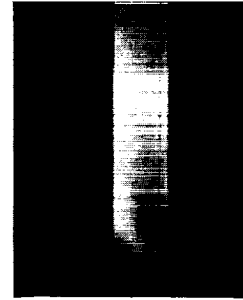


Figure 12. Velocity Trajectories for Single Row of Jets

S/D = 2 , H/D = 8



J = 72



J = 8



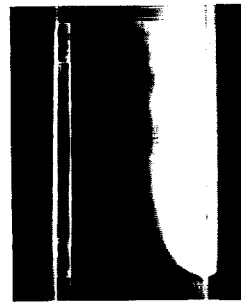
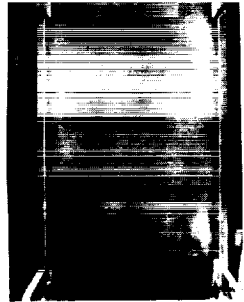
S/D = 2 , H/D = 24

SIDE VIEW



J = 72

TOP VIEW



J = 8



Figure 13. Smoke Photographs of Single Row of Jets

S/D = 4 , H/D = 8

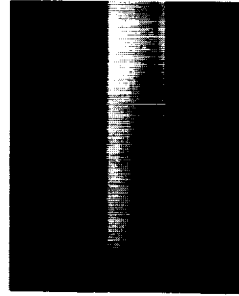
S/D = 4 , H/D = 24

SIDE VIEW

TOP VIEW



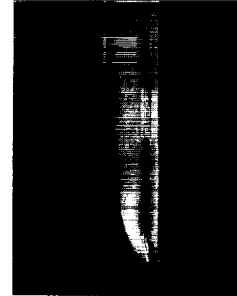
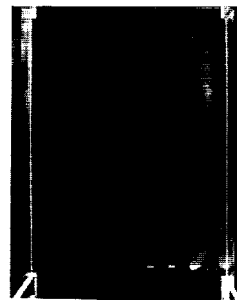
J = 72



J = 72



J = 8



J = 8

Figure 14. Smoke Photographs of Single Row of Jets

S/D = 6 , H/D = 8



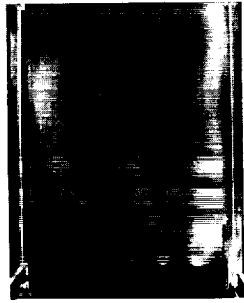
J = 72



J = 8

S/D = 6 , H/D = 24

TOP VIEW



J = 72



J = 8

SIDE VIEW



Figure 15. Smoke Photographs of Single Row of Jets

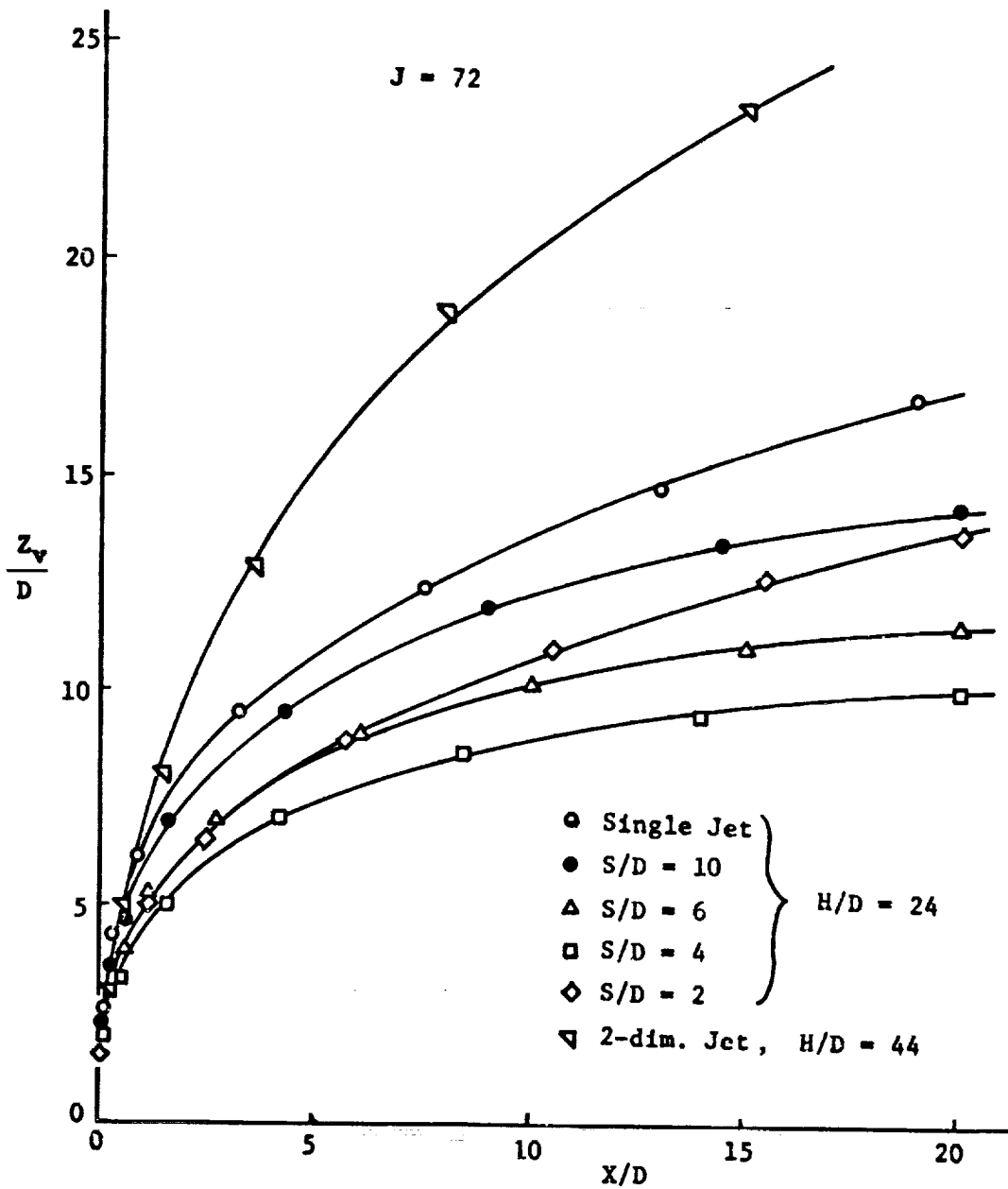


Figure 16. Effect of Spacing Ratio on Jet Trajectories

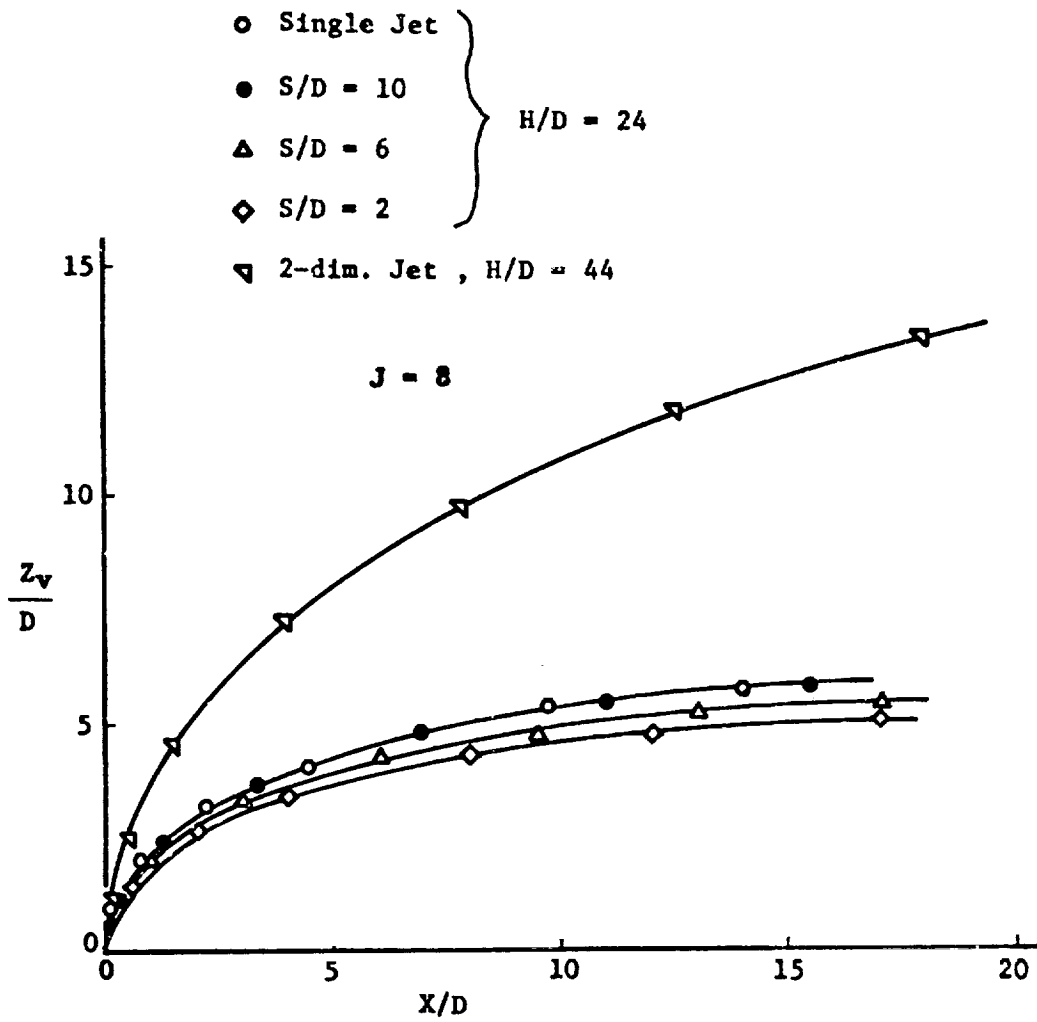


Figure 17. Effect of Spacing Ratio on Jet Trajectories

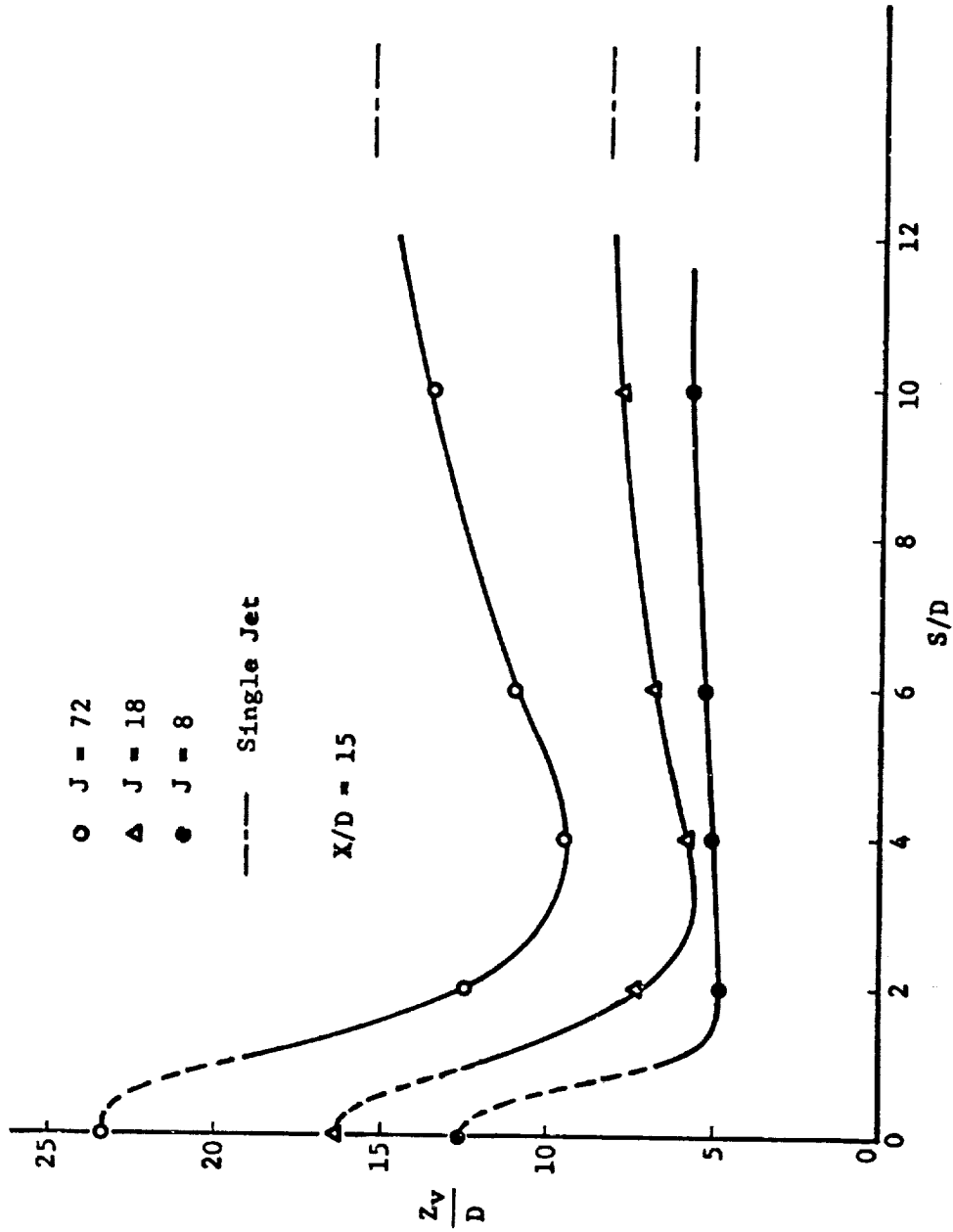


Figure 18. Change of Jet Centerline Location with Spacing Ratio

$J = 72$  ,  $S/D = 2$  ,  $H/D = 24$

$X/D = 2$

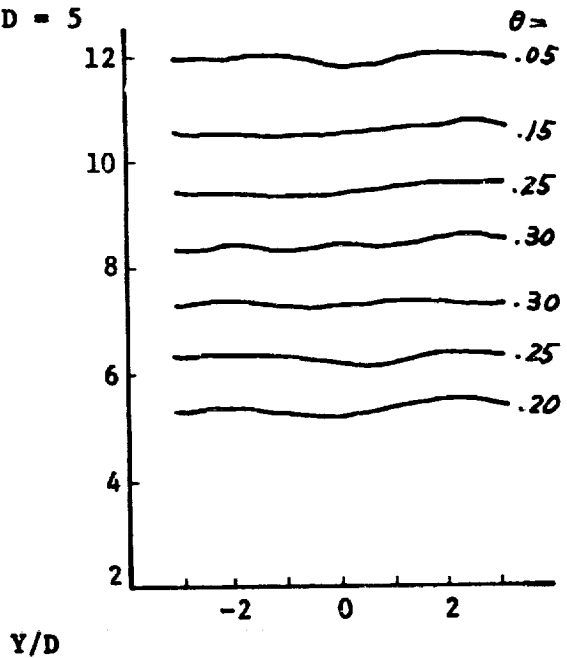
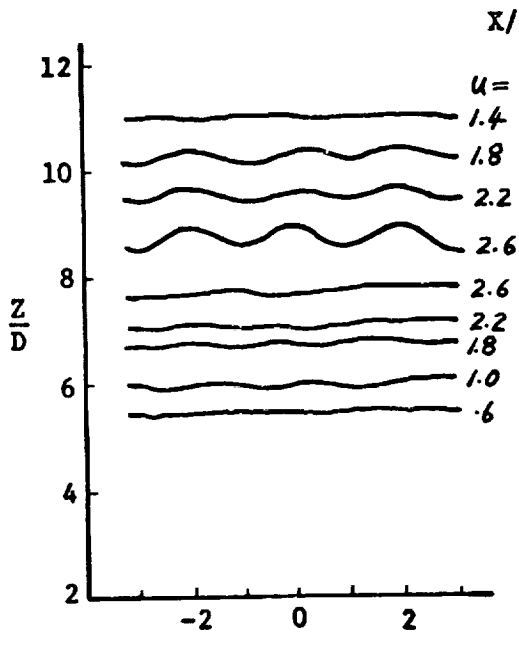
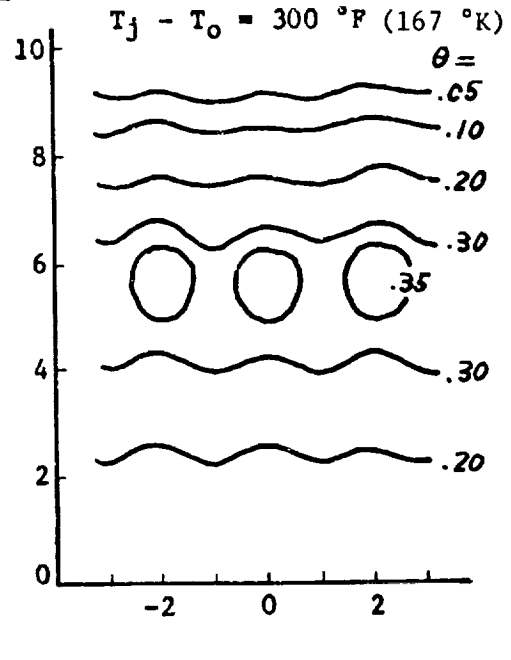
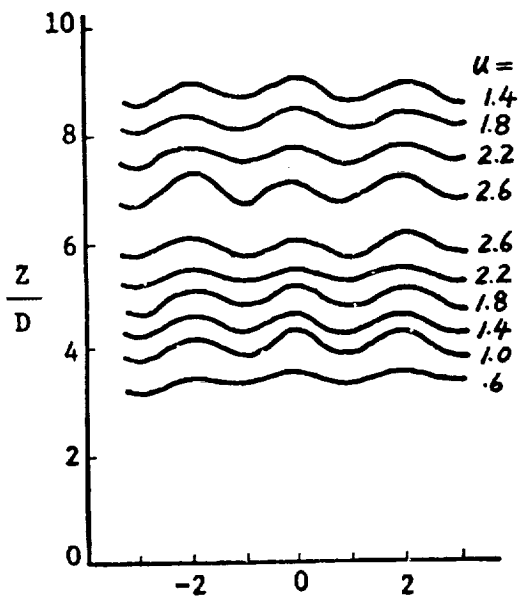


Figure 19. Contours of Constant Speed and Temperature for Single Row of Jets

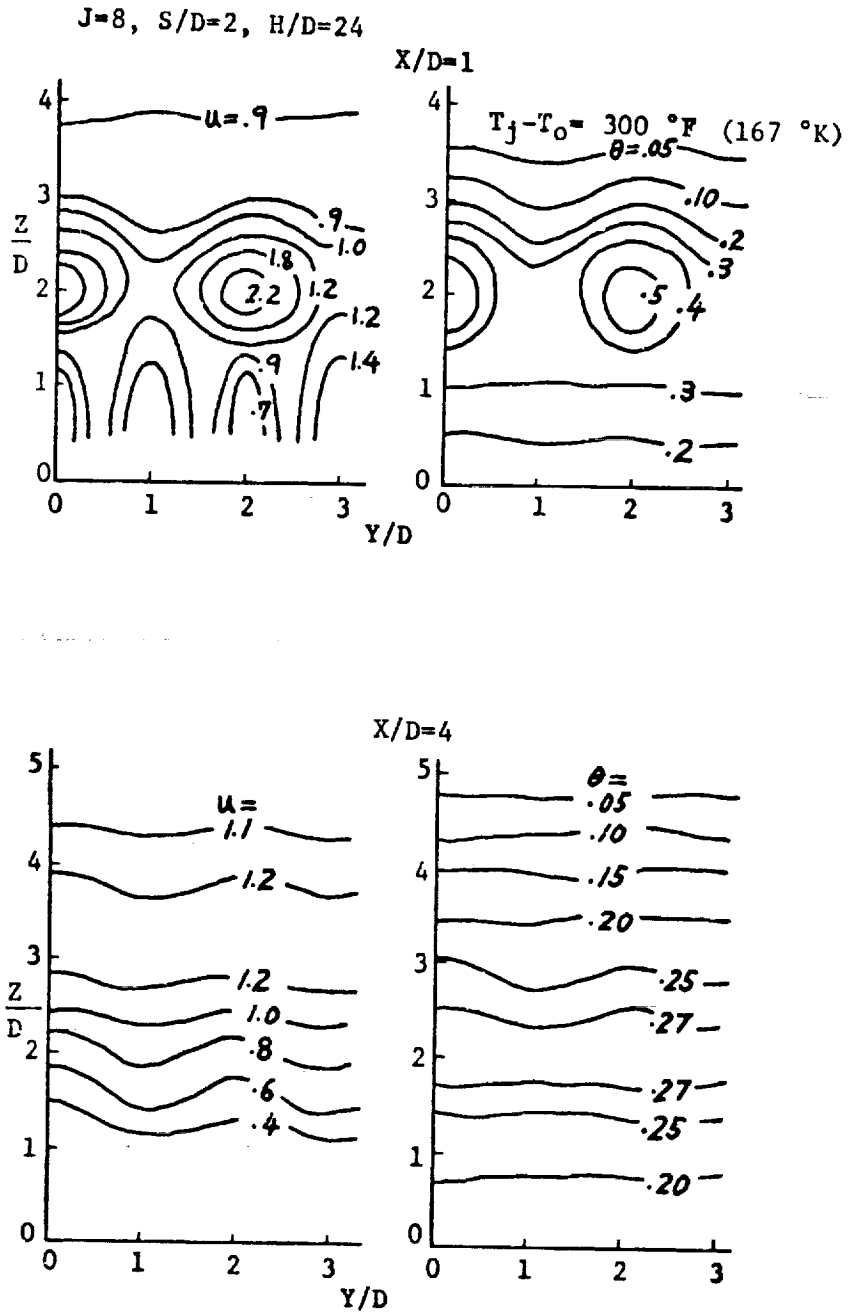


Figure 20. Contours of Constant Speed and Temperature for Single Row of Jets

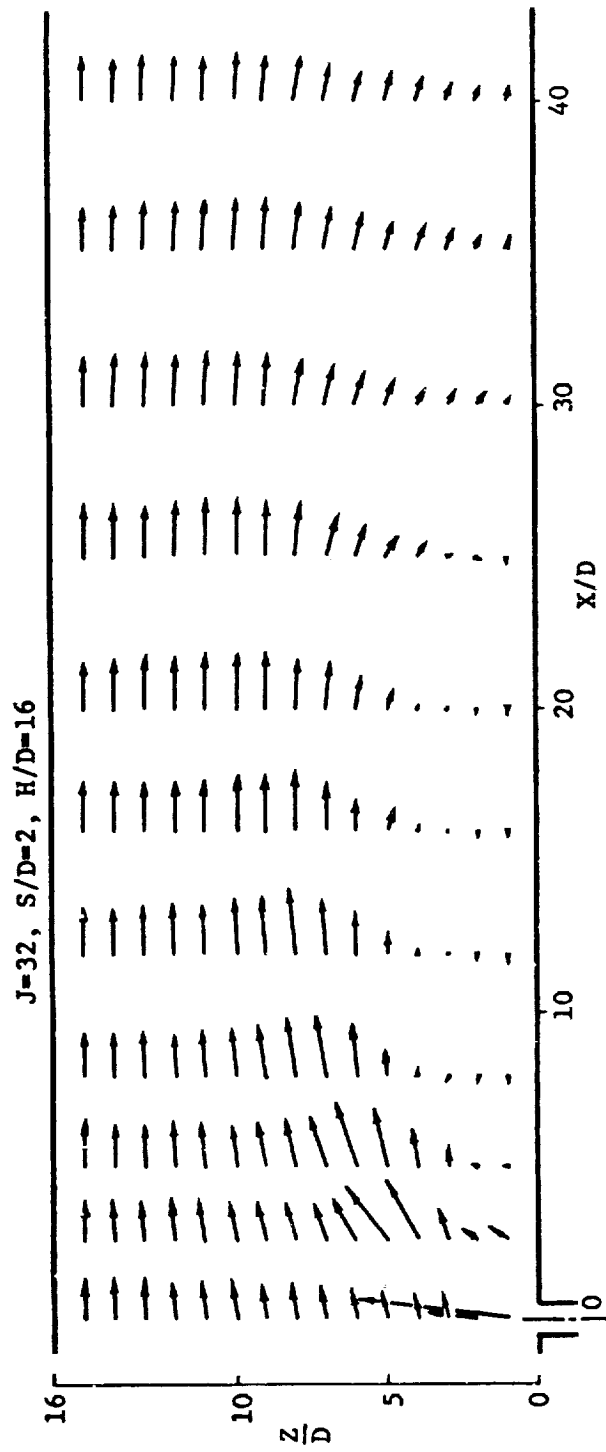


Figure 21. Distribution of Velocity Vectors in the Plane of Symmetry for Single Row of Jets

J = 72 , S/D = 4 , H/D = 24

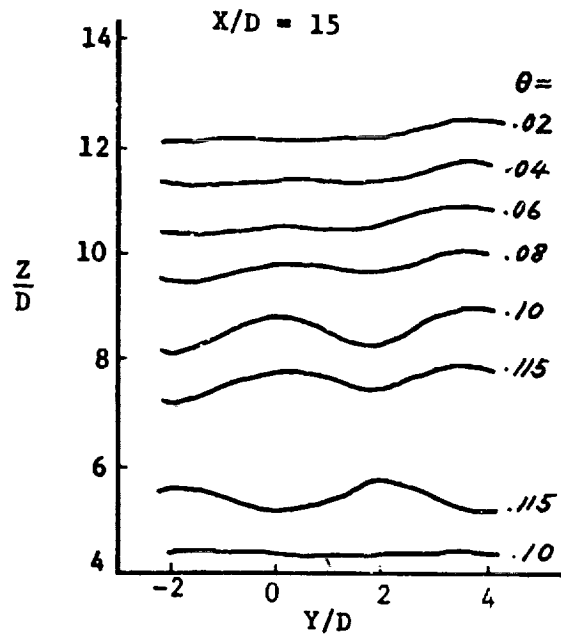
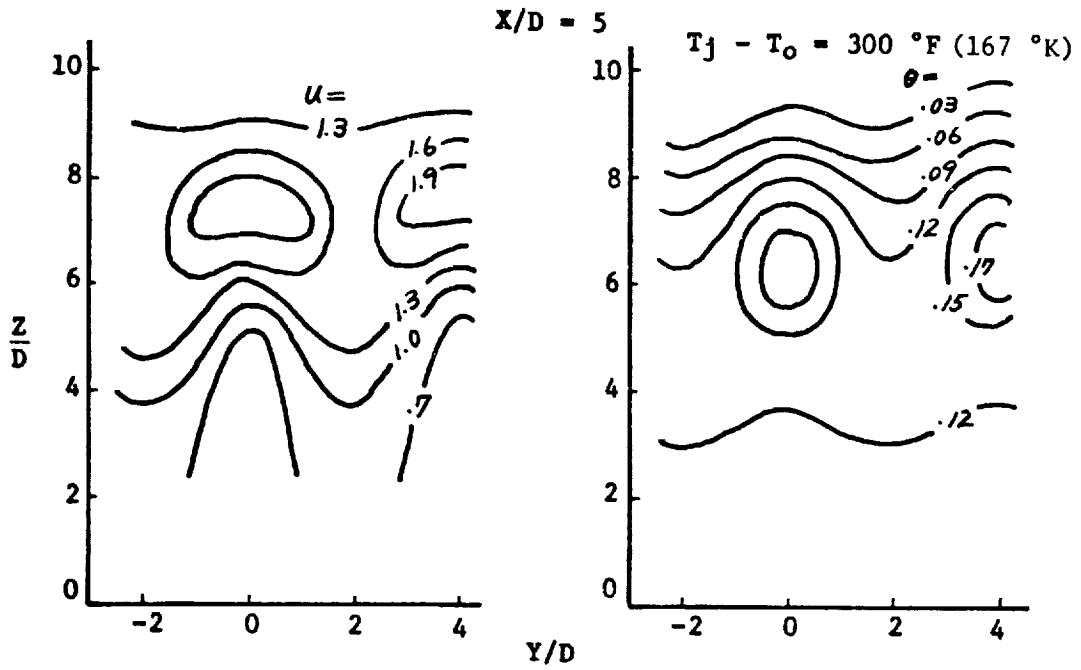


Figure 22. Contours of Constant Speed and Temperature for Single Row of Jets

$J = 8, S/D = 4, H/D = 24$

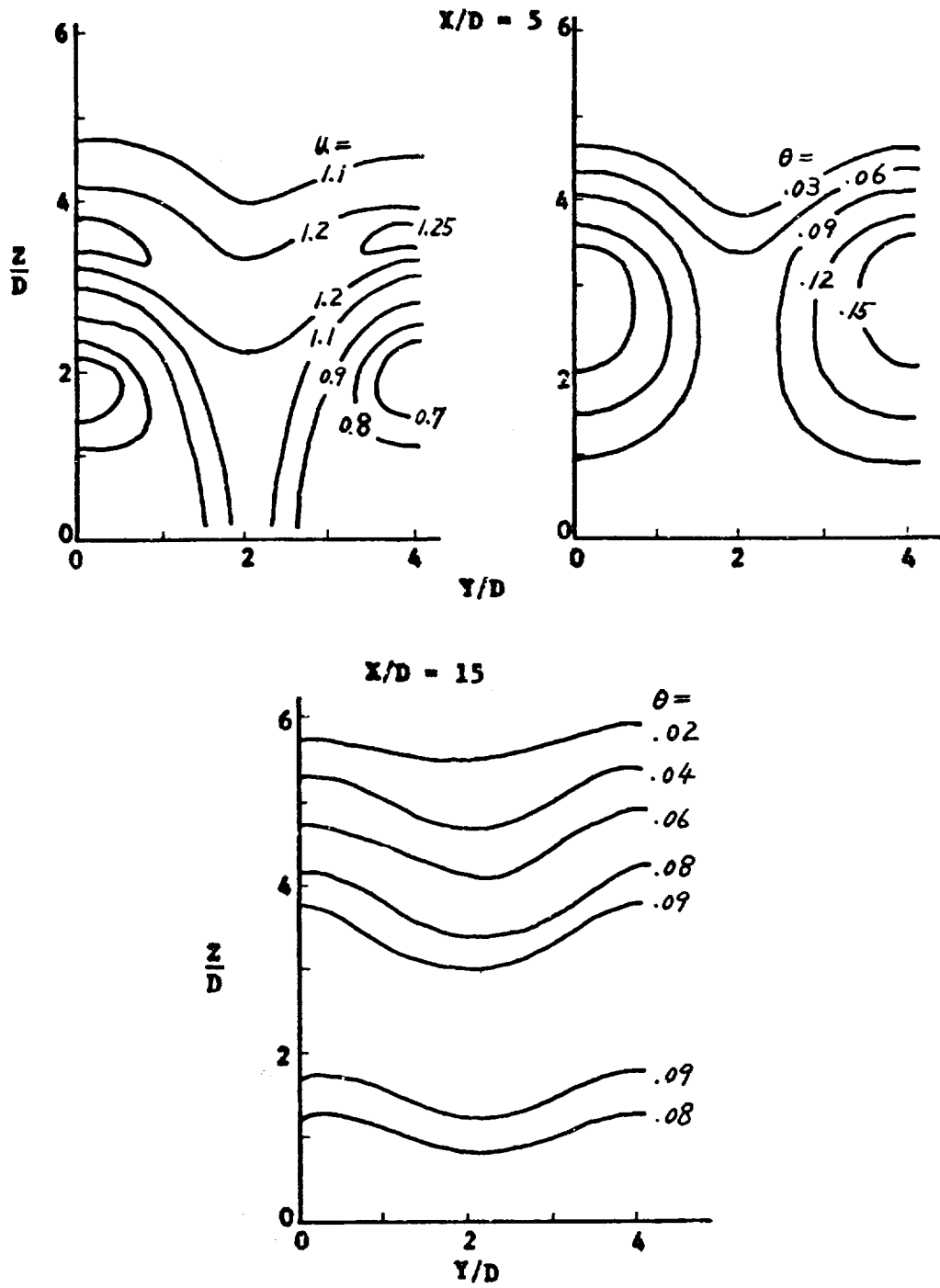


Figure 23. Contours of Constant Speed and Temperature for Single Row of Jets

$J = 72$  ,  $S/D = 6$  ,  $H/D = 24$

$X/D = 5$

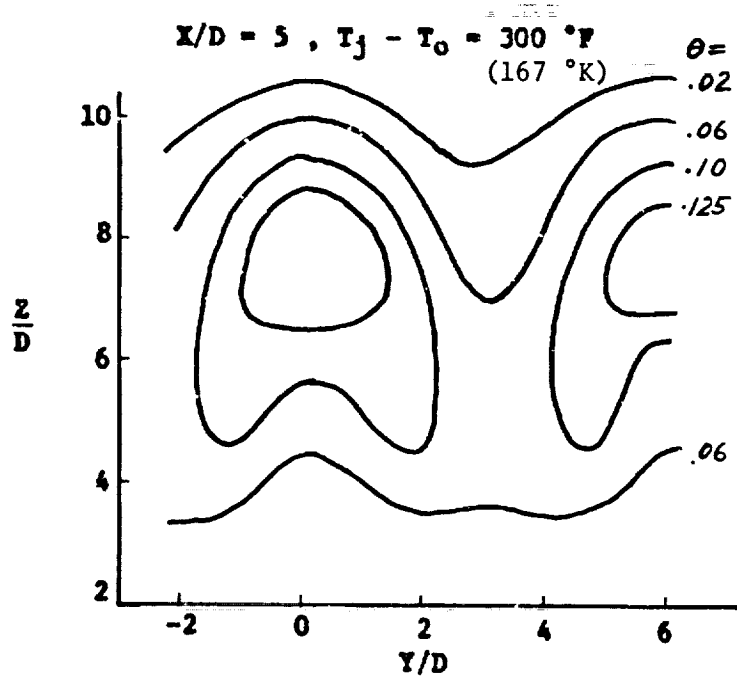
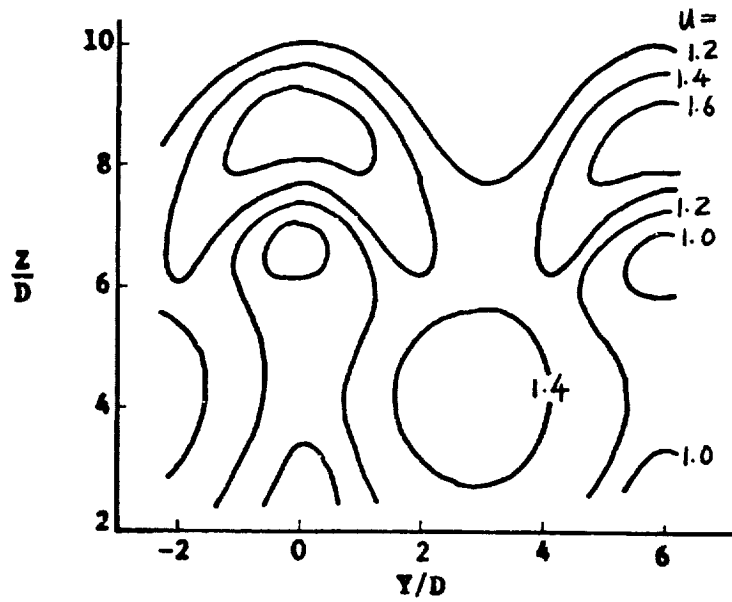


Figure 24. Contours of Constant Speed and Temperature for Single Row of Jets

$J = 72$  , Single Jet ,  $H/D = 12$

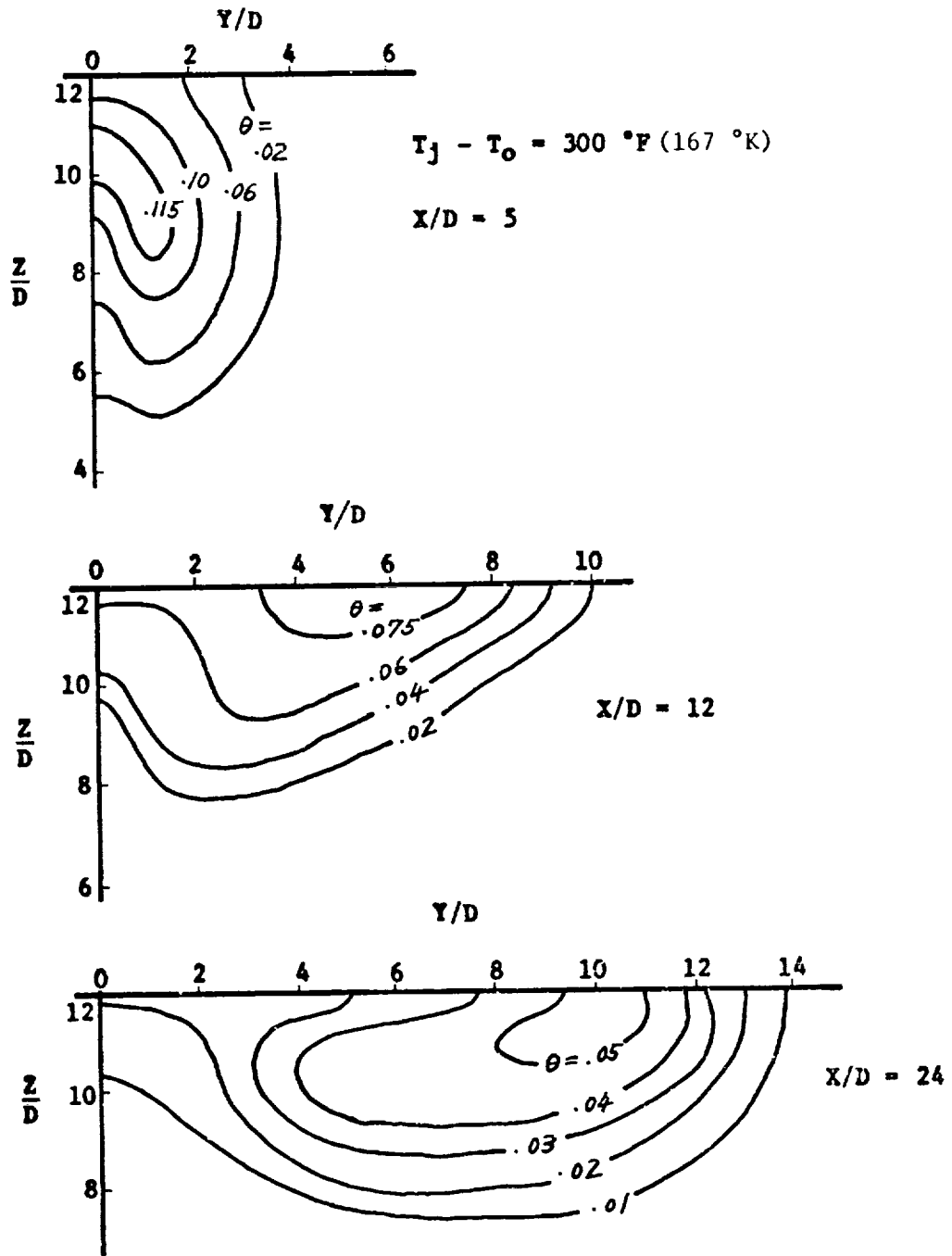


Figure 25. Contours of Constant Temperature for Single Jet

$J = 72$  ,  $H/D = 12$  ,  $X/D = 12$

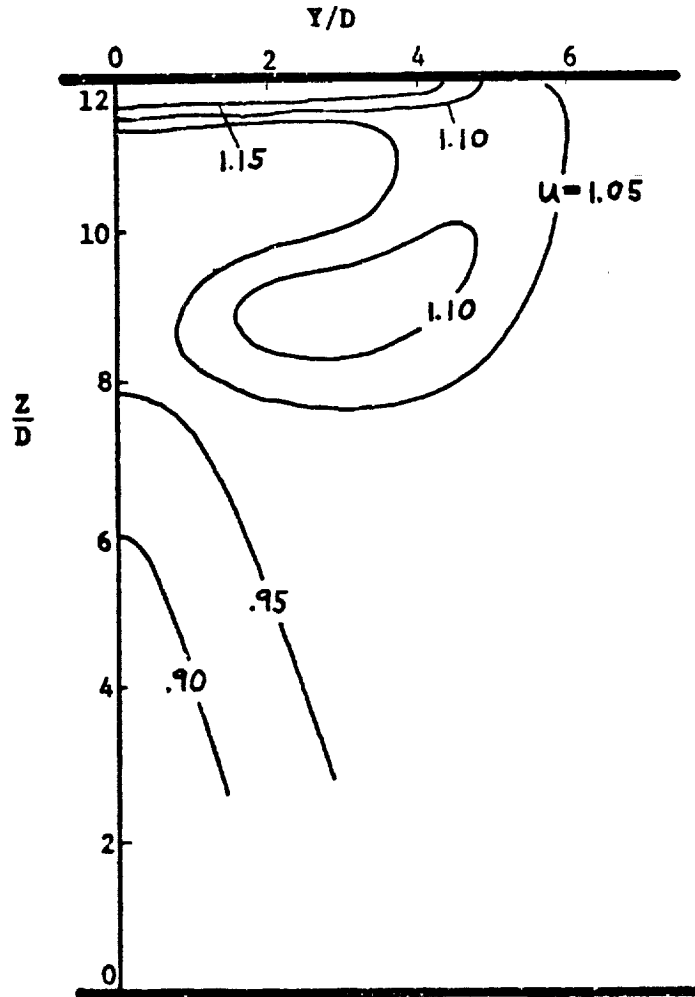
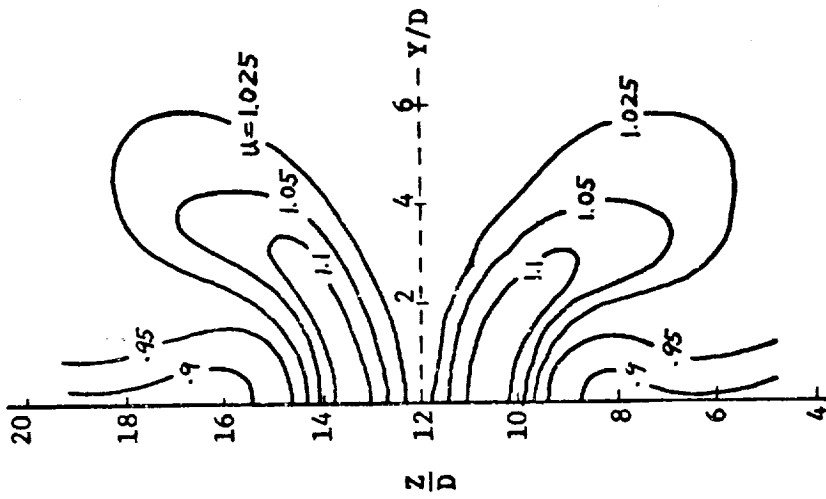


Figure 26. Contours of Constant Speed for Single Jet

$J = 32$ ,  $H/D = 12$ ,  $X/D = 12$

Two Opposing Jets



Single Jet with Opposing Wall

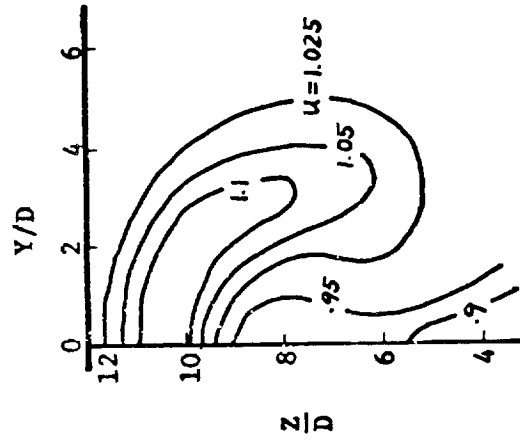


Figure 27. Contours of Constant Speed for Two Opposing Jets

$S/D = 2$  ,  $H/D = 24$  ,  $T_j - T_o = 300$  °F (167 °K)

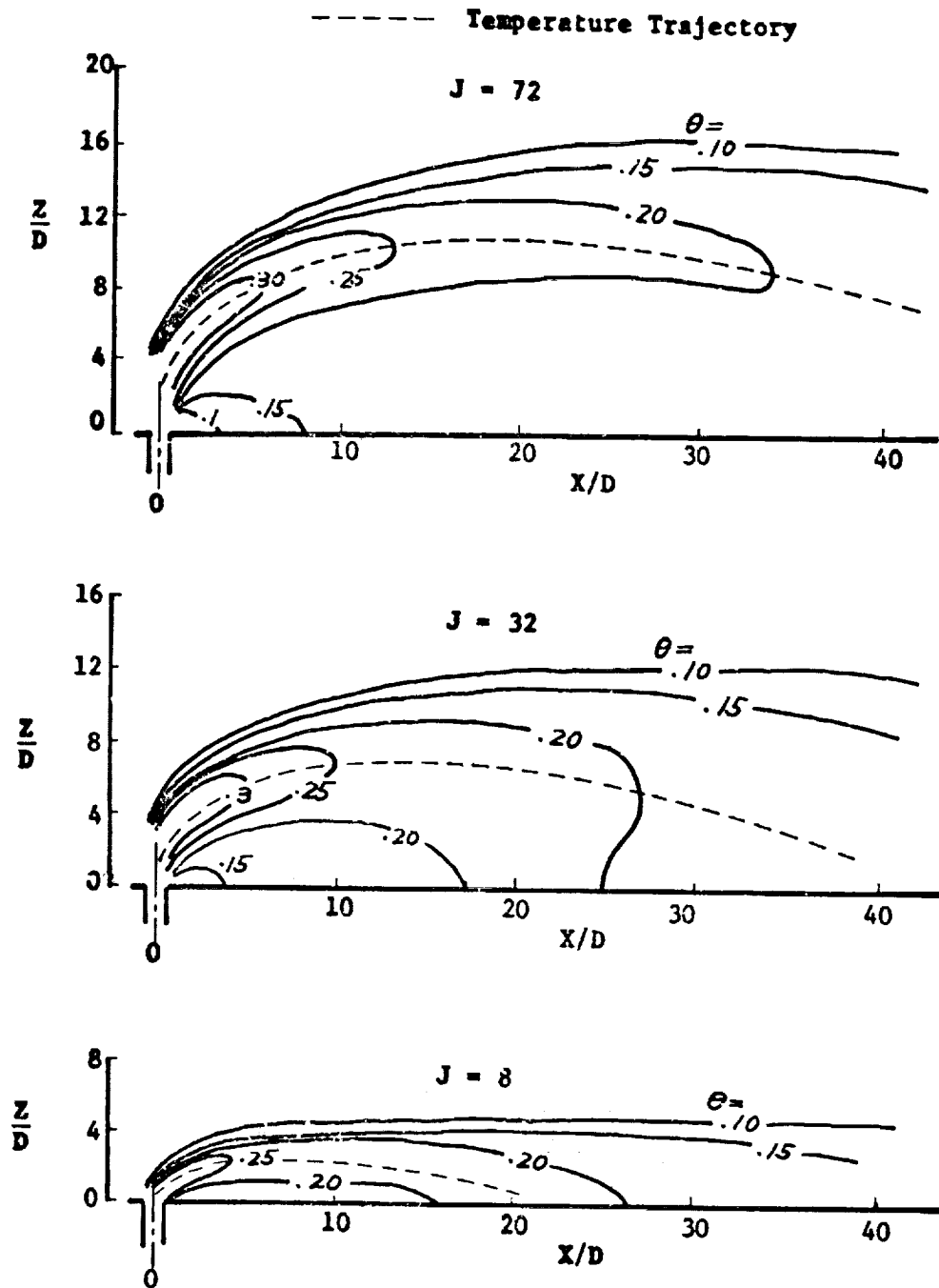


Figure 28. Temperature Distributions in the Plane of Symmetry for Single Row of Jets

$J = 32$  ,  $S/D = 2$  ,  $T_j - T_0 = 300$  °F (167 °K)

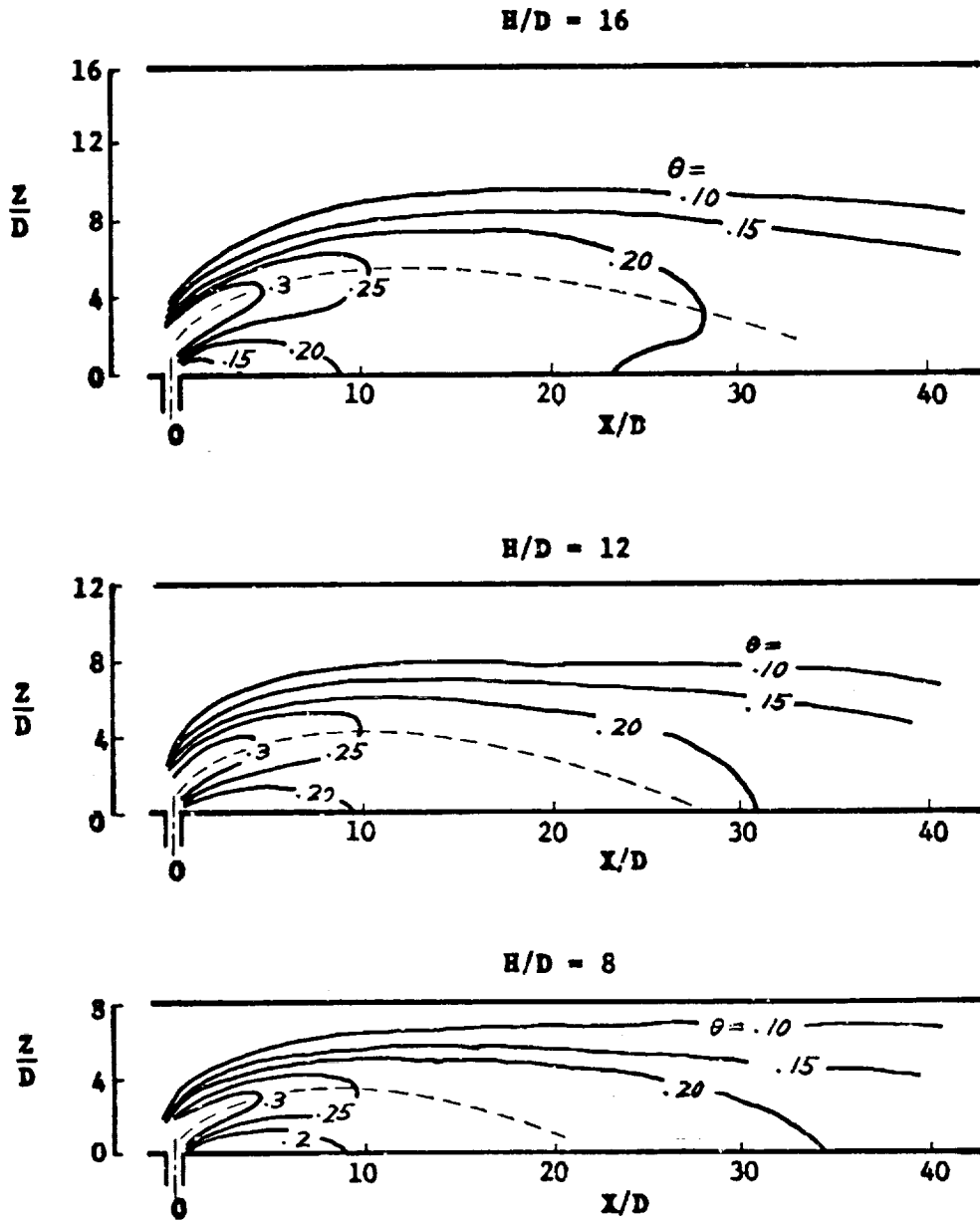


Figure 29. Temperature Distributions in the Plane of Symmetry for Single Row of Jets

$S/D = 4$  ,  $H/D = 24$  ,  $T_j - T_o = 300$  °F (167 °K)

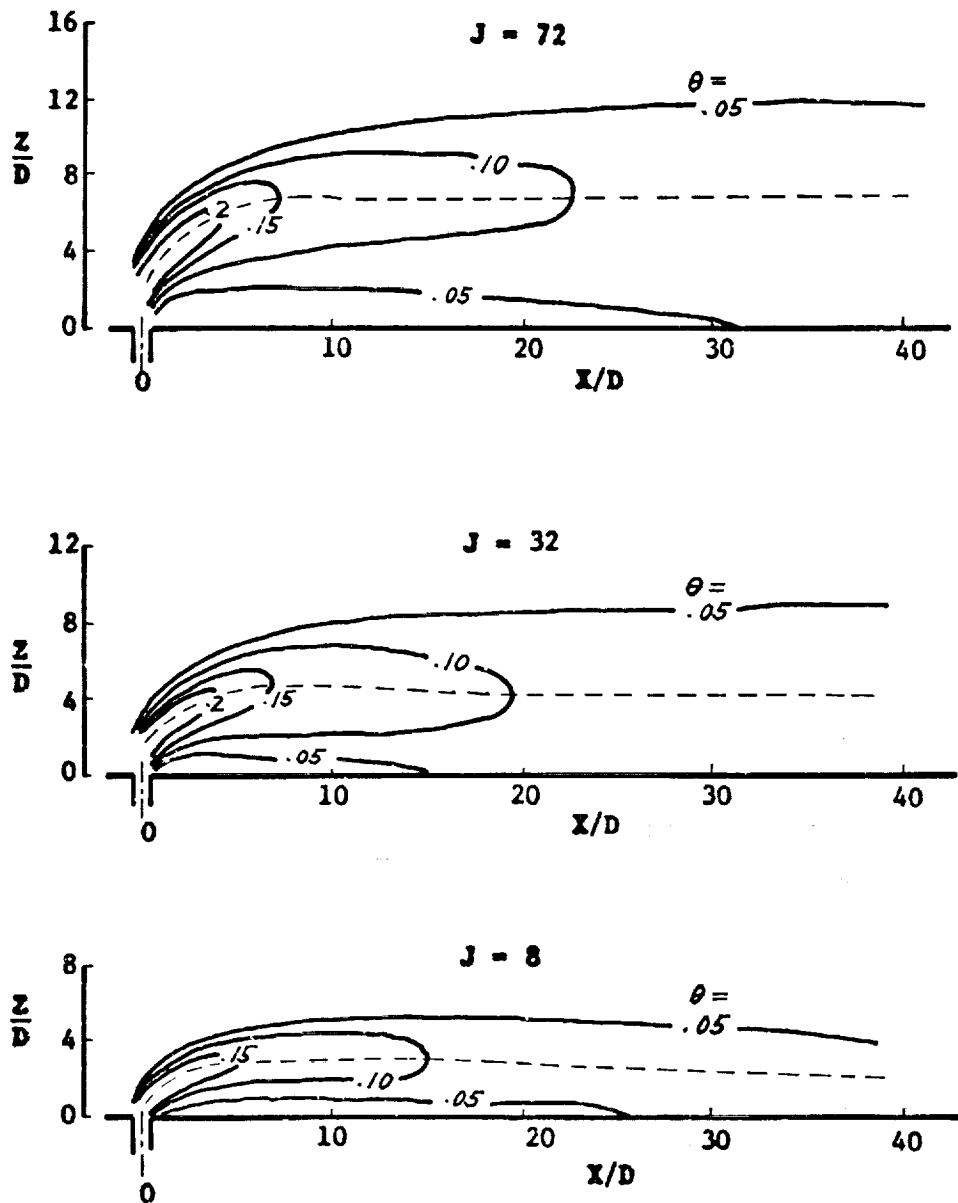


Figure 30. Temperature Distributions in the Plane of Symmetry for Single Row of Jets

$J = 32$  ,  $S/D = 4$  ,  $T_j - T_o = 300 \text{ }^\circ\text{F}$  ( $167^\circ\text{K}$ )

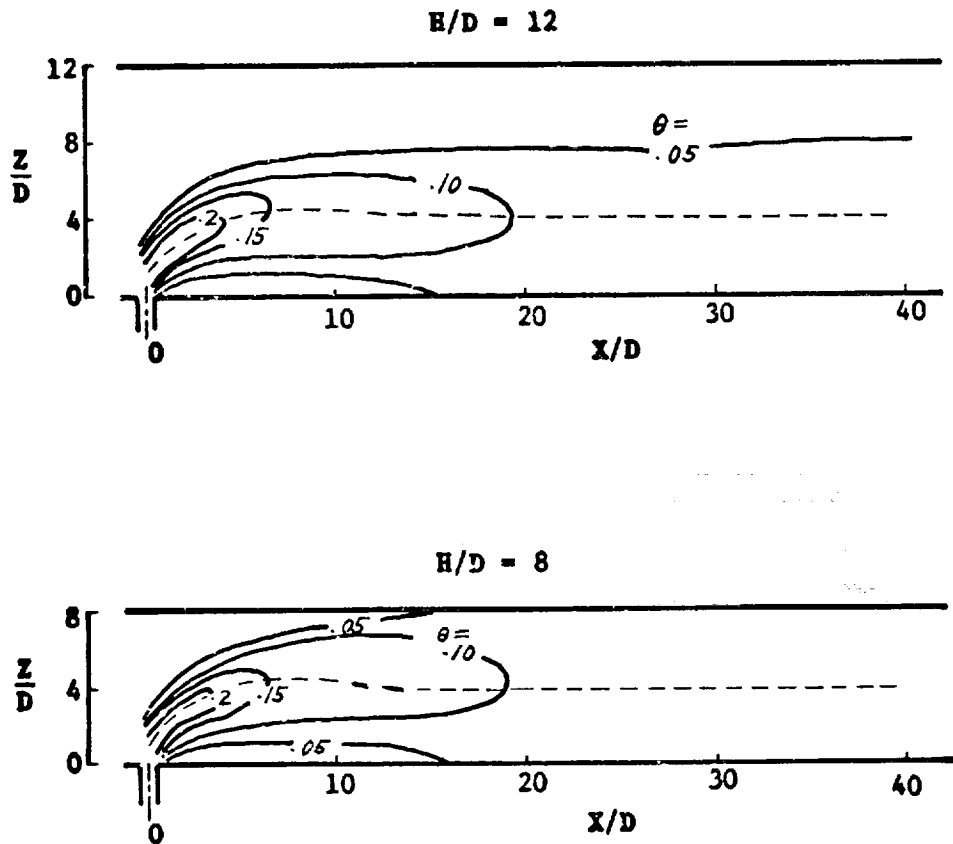


Figure 31. Temperature Distributions in the Plane of Symmetry for Single Row of Jets

$S/D = 6$  ,  $H/D = 24$  ,  $T_j - T_o = 300$  °F (167 °K)

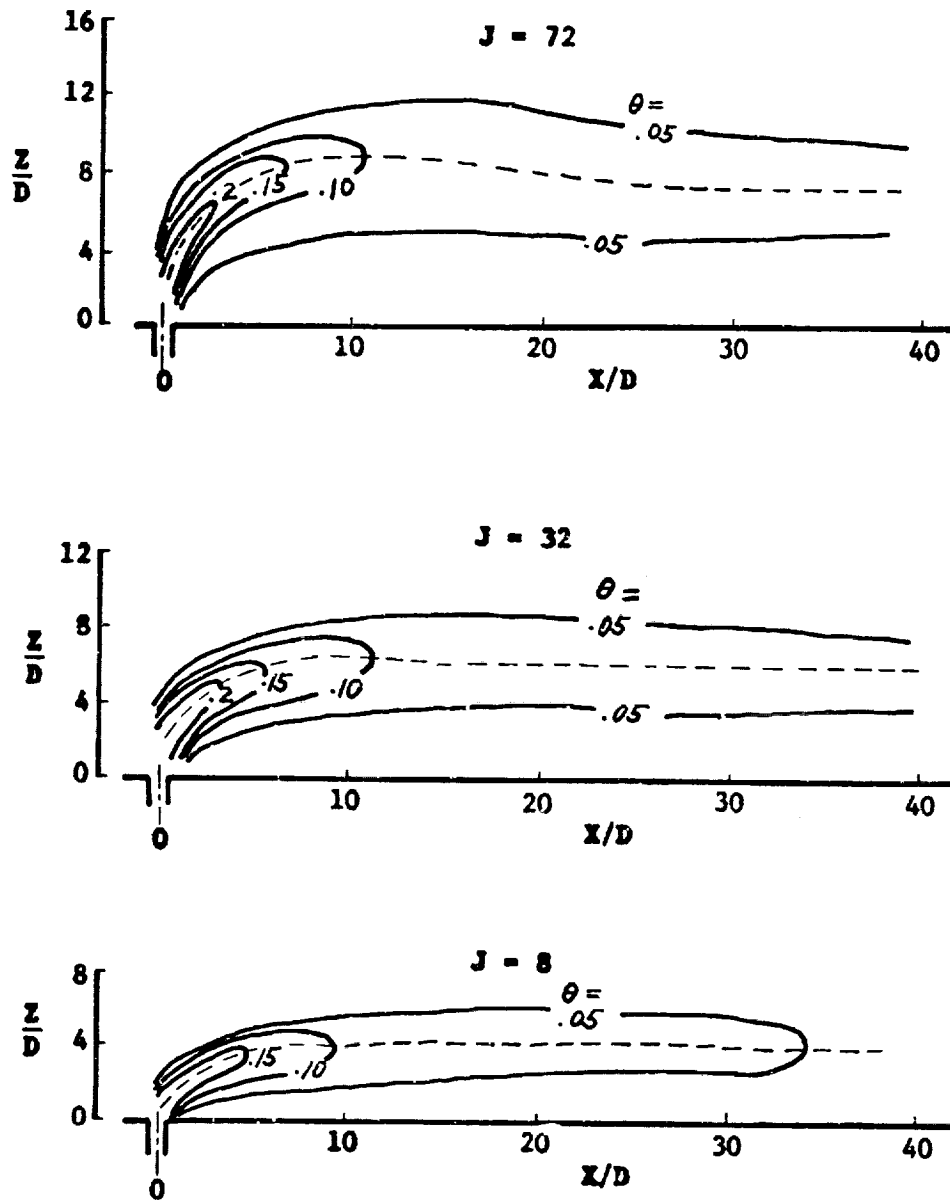


Figure 32. Temperature Distributions in the Plane of Symmetry for Single Row of Jets

Single Jet ,  $H/D = 24$  ,  $T_j - T_o = 300 \text{ }^\circ\text{F}$  (167  $^\circ\text{K}$ )

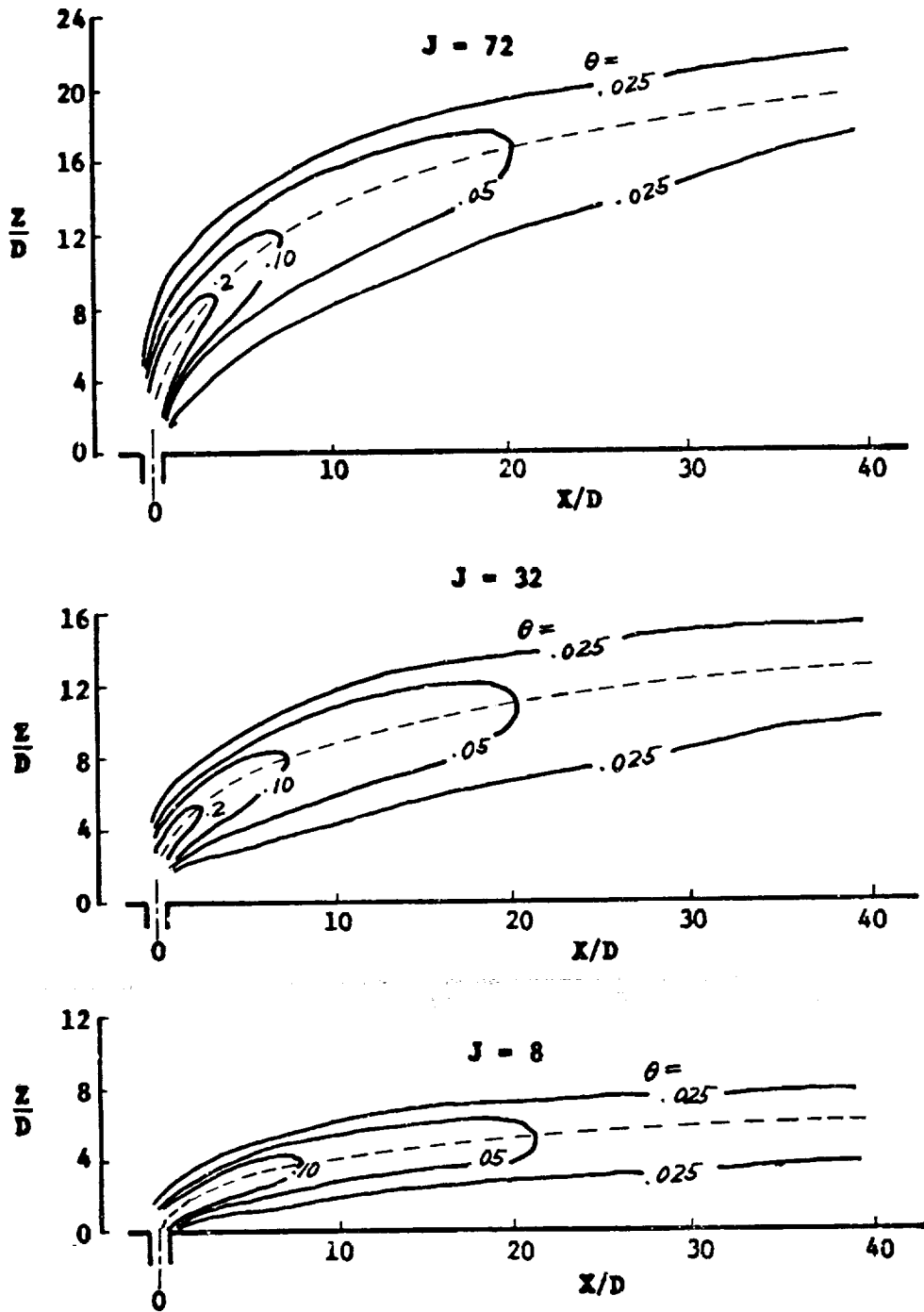


Figure 33. Temperature Distributions in the Plane of Symmetry for Single Jet

J = 32 , Single Jet ,  $T_j - T_o = 300$  °F (167 °K)

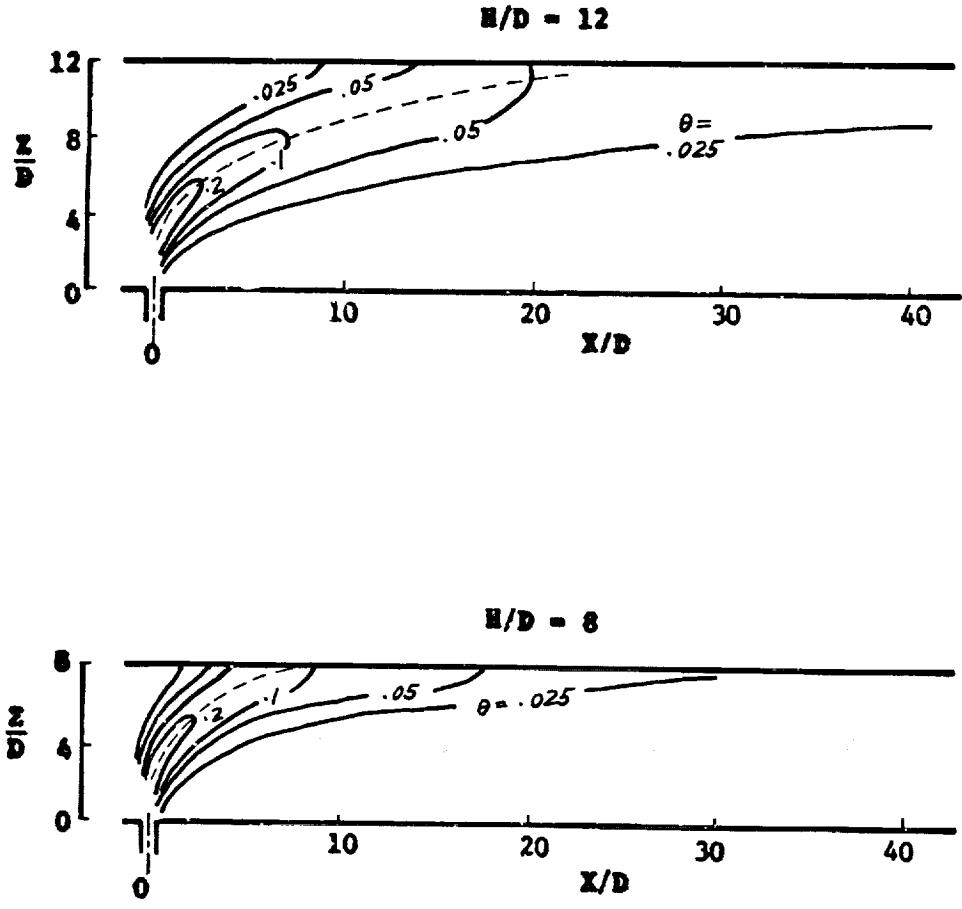


Figure 34. Temperature Distributions in the Plane of Symmetry for Single Jet

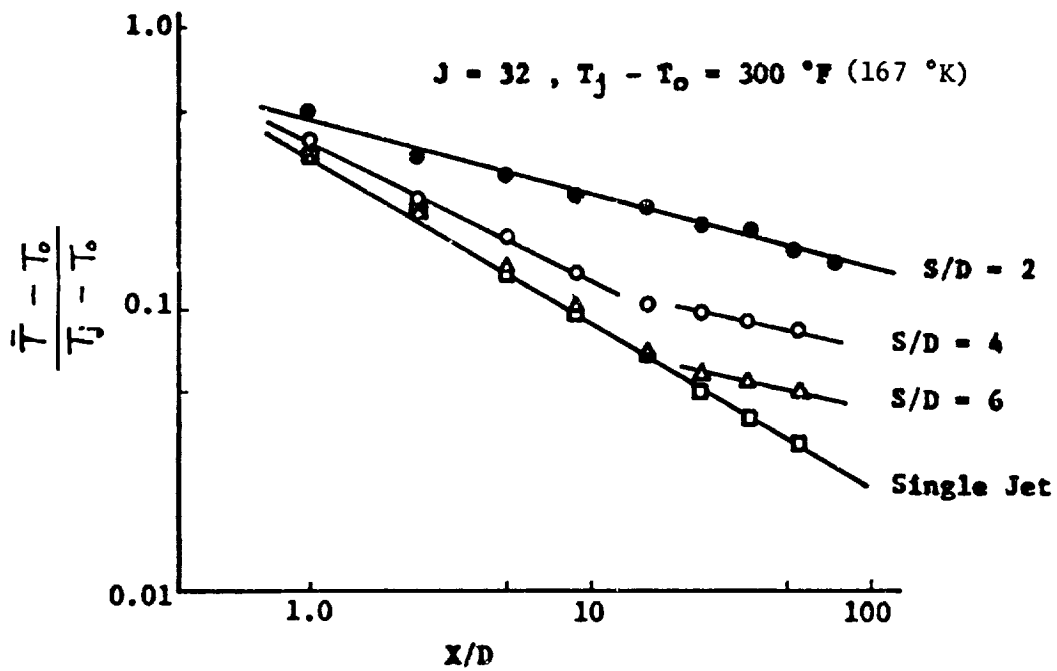
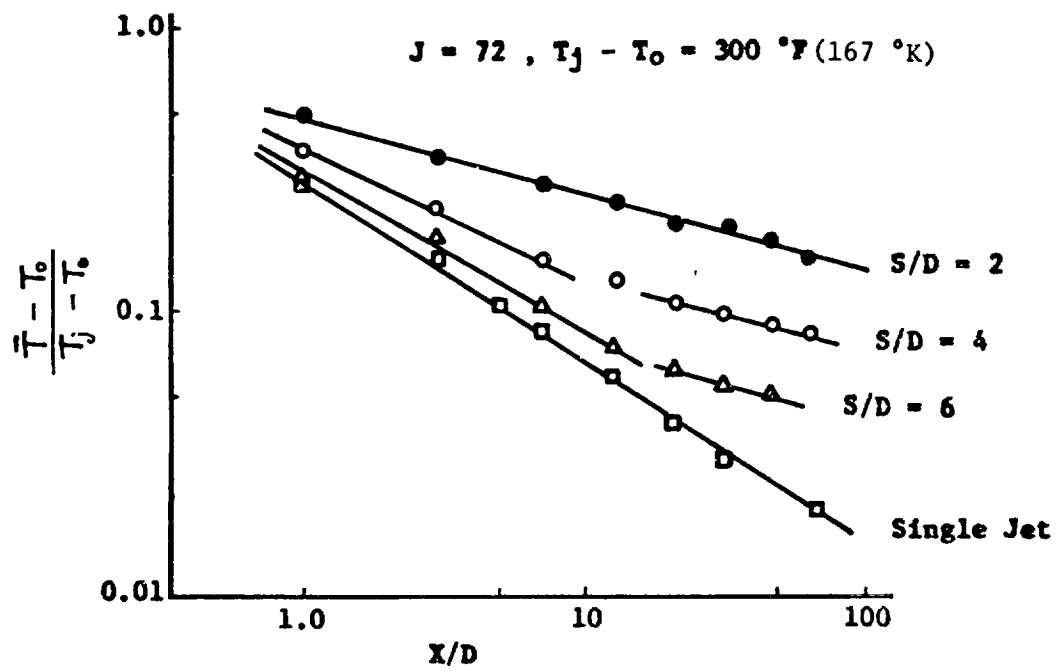


Figure 35. Decay of Centerline Temperature for Single Row of Jets

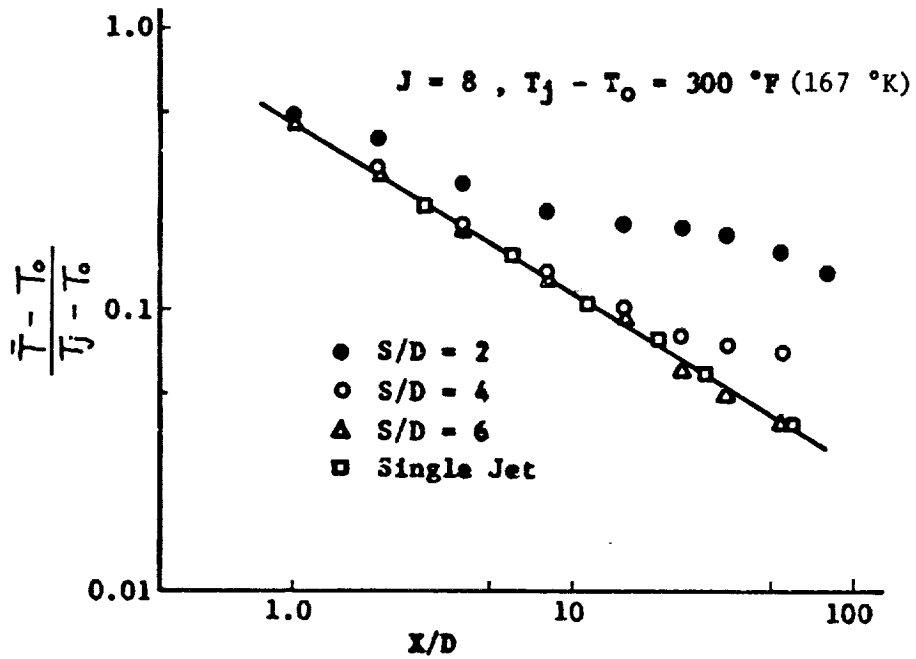
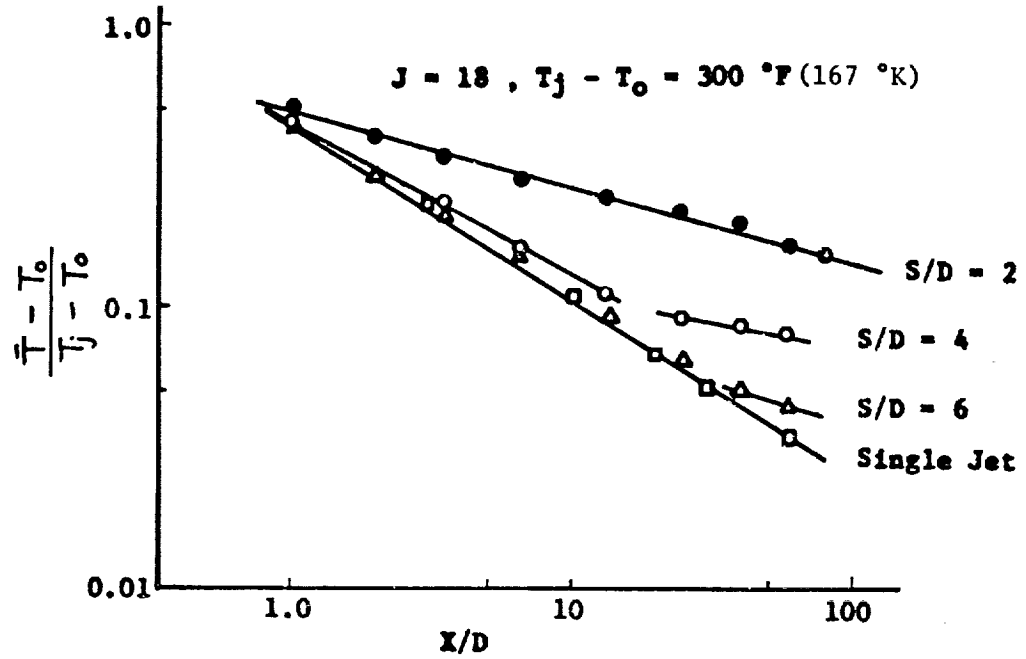


Figure 36. Decay of Centerline Temperature for Single Row of Jets

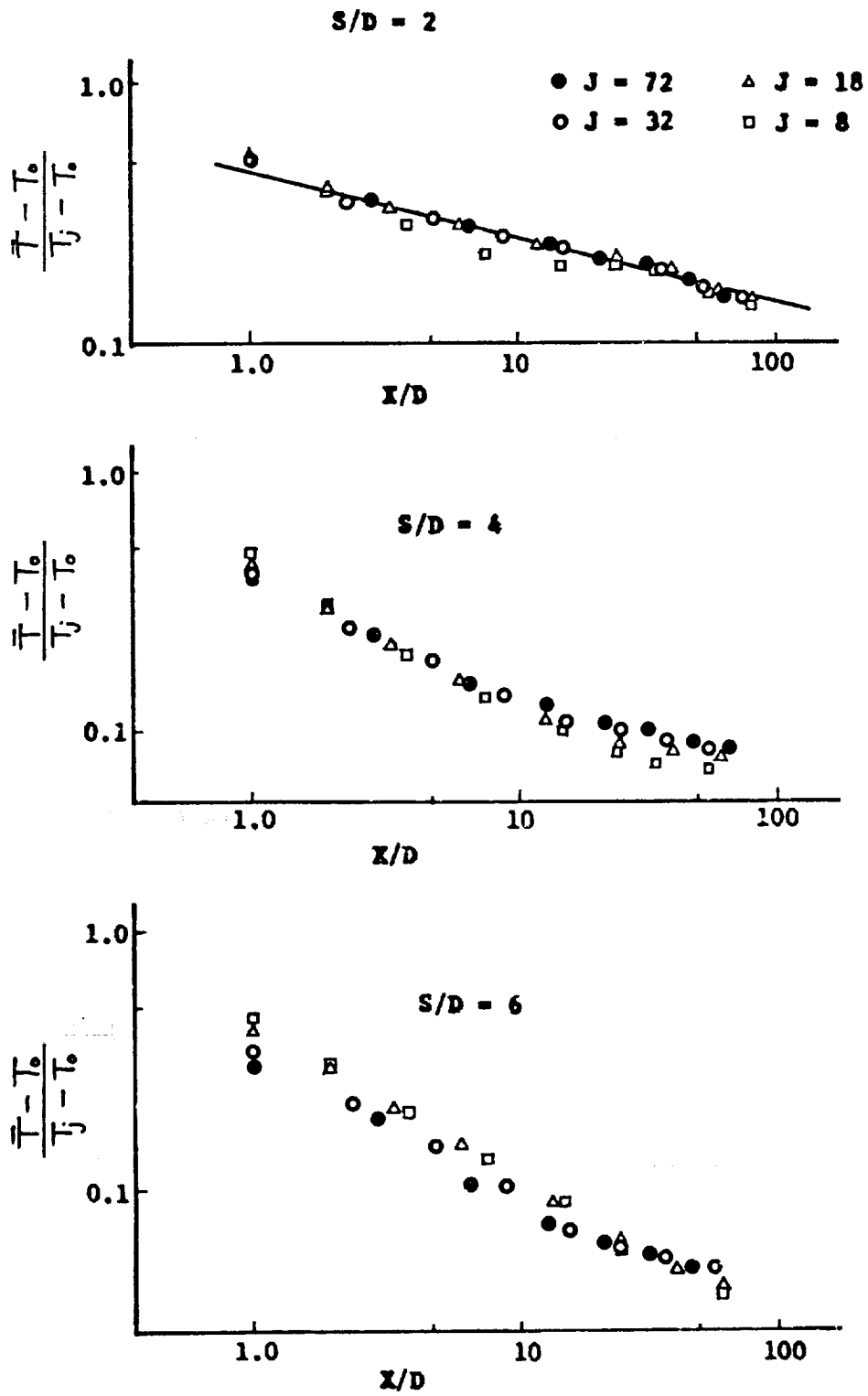
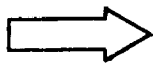


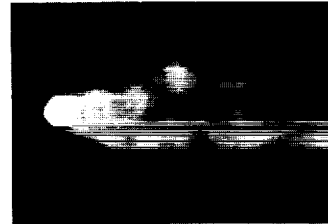
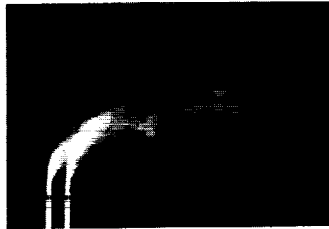
Figure 37. Decay of Centerline Temperature for Single Row of Jets



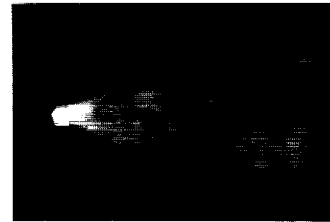
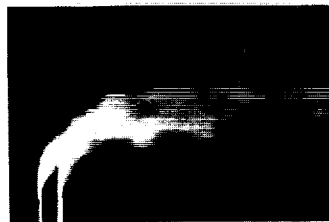
S/D = 4

SIDE VIEW

TOP VIEW



J = 70



J = 40



J = 10

Figure 38. Smoke Photographs of Multiple Jets

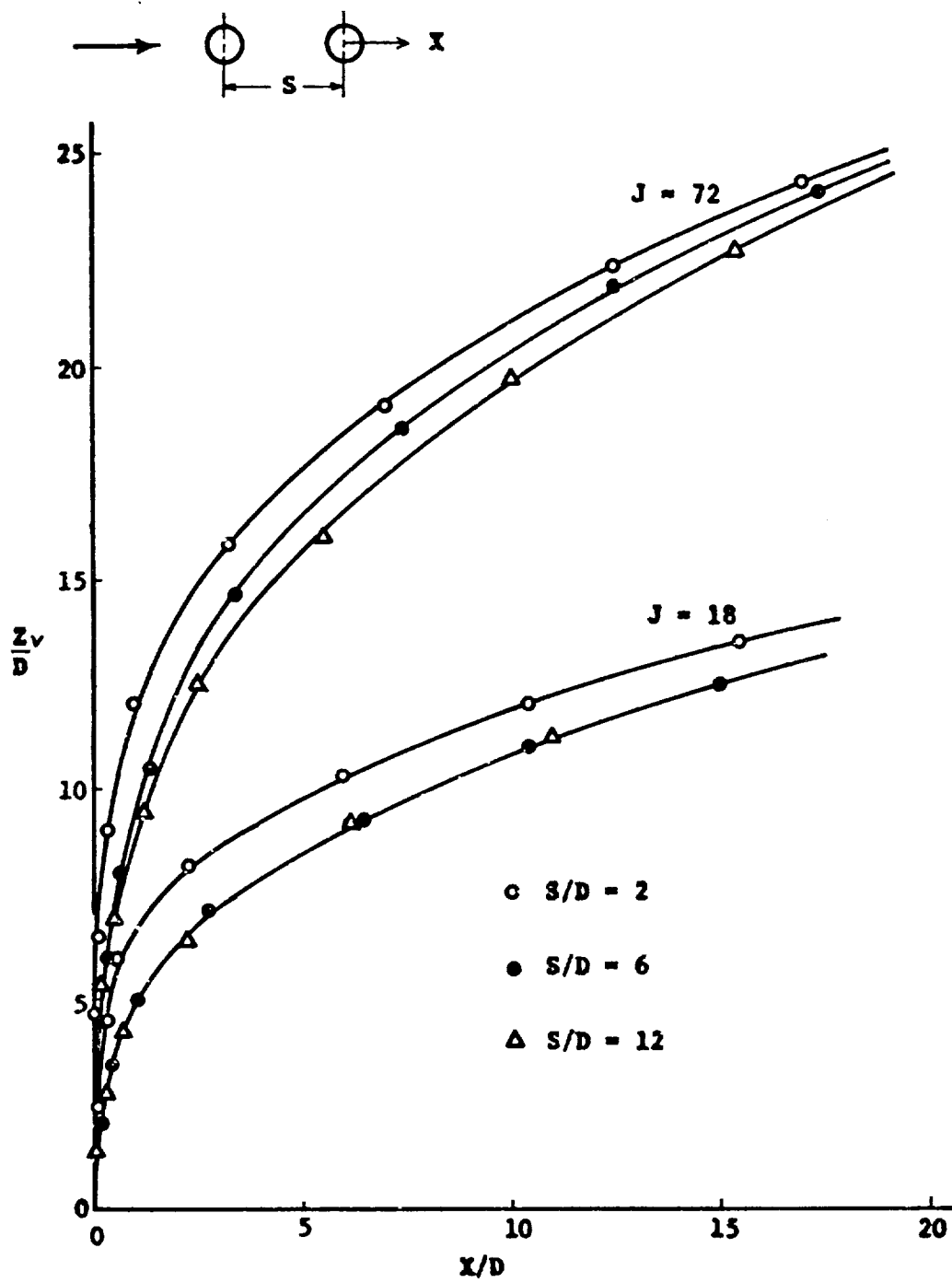


Figure 39. Velocity Trajectories for Multiple Jets

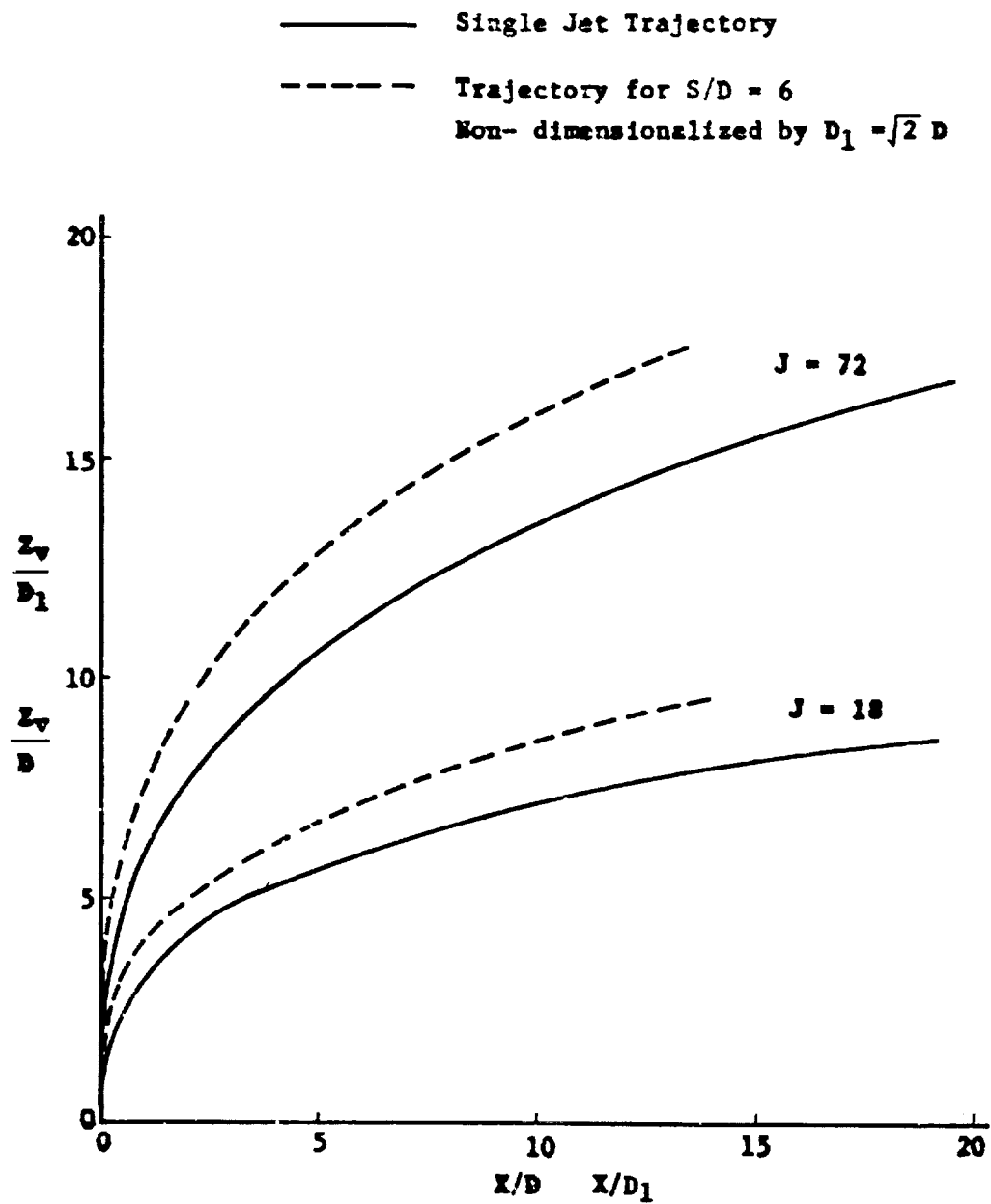


Figure 40. Comparison of Jet Trajectories

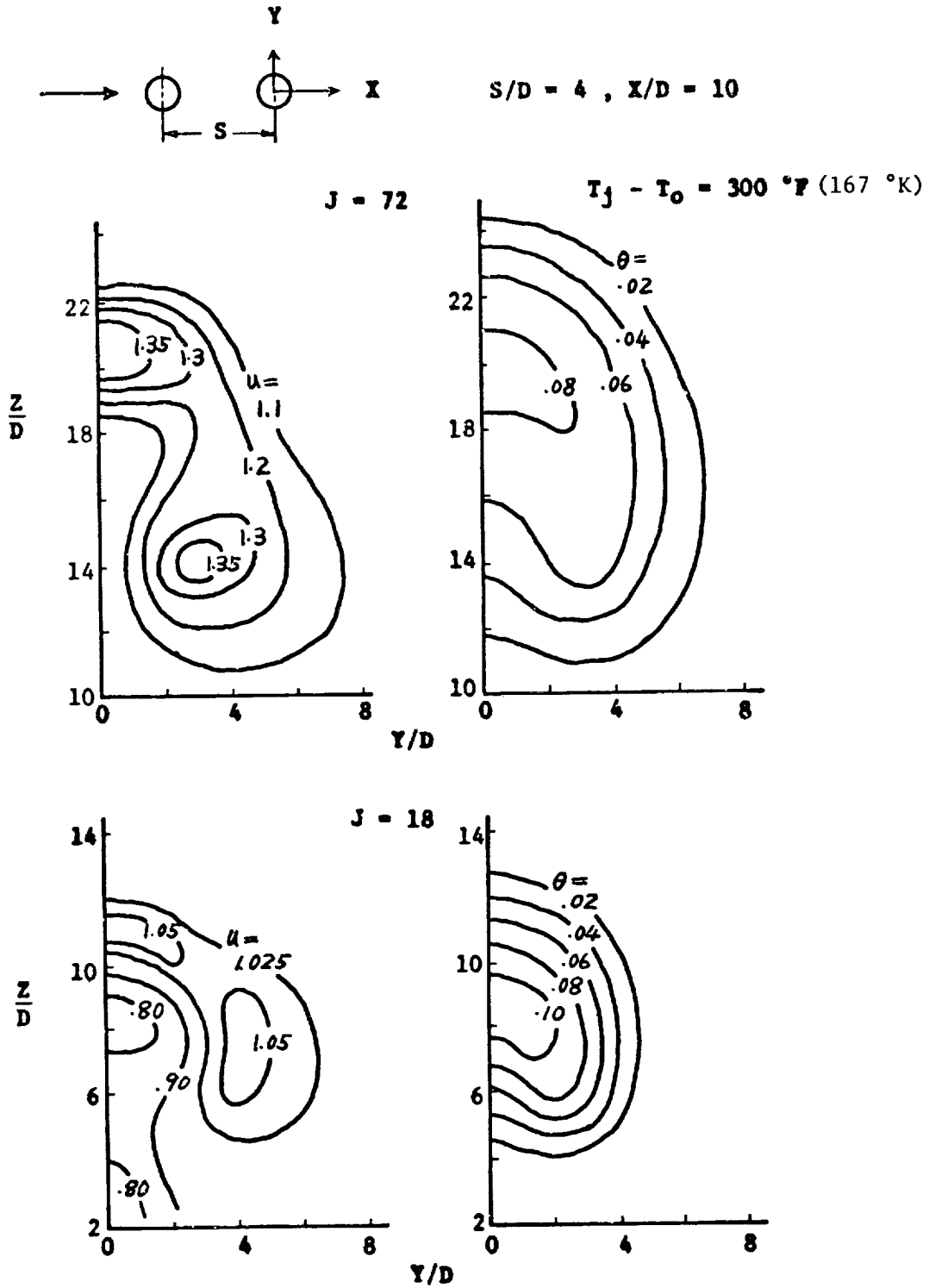


Figure 41. Contours of Constant Speed and Temperature for Multiple Jets

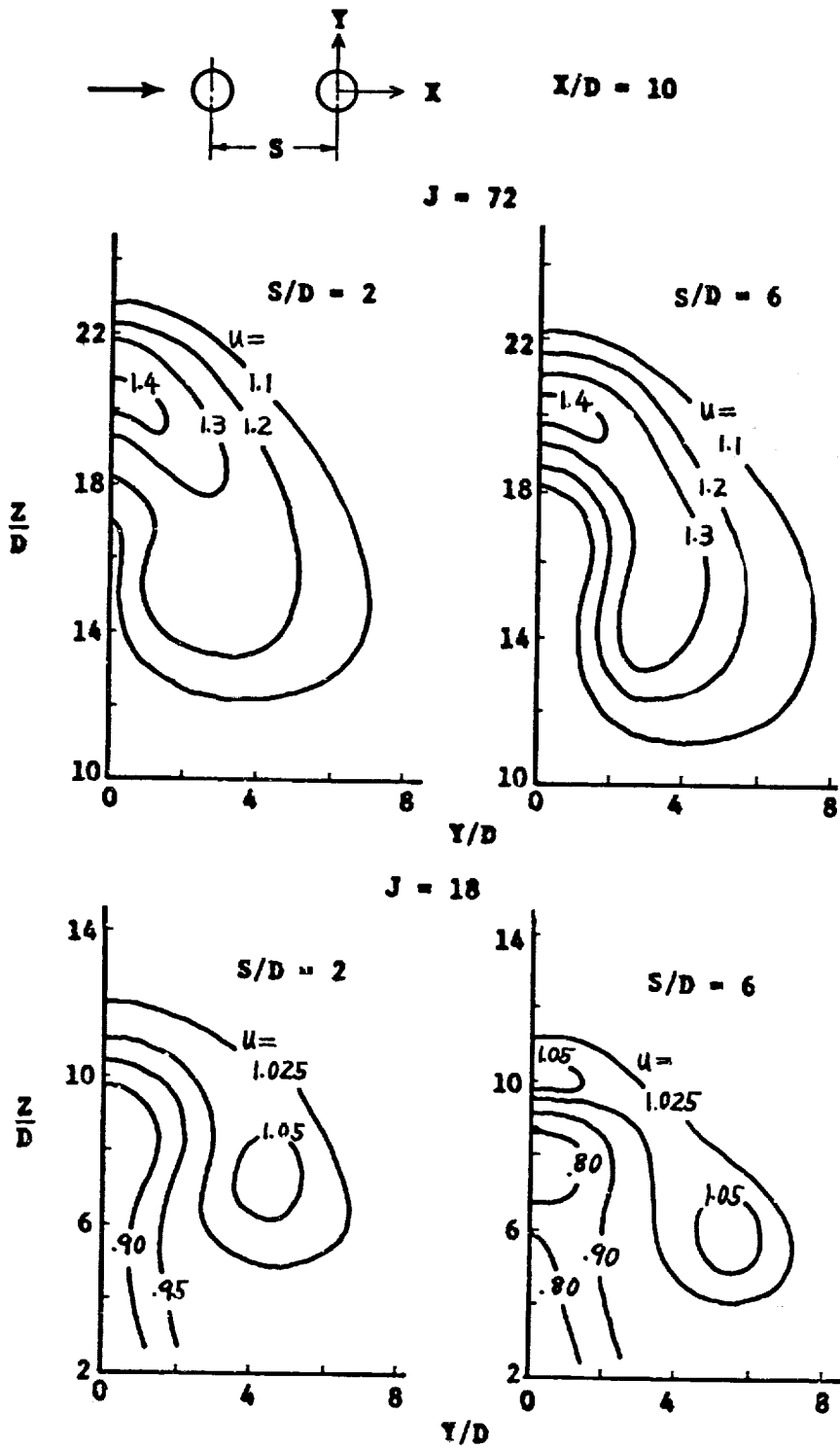
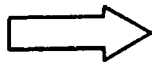


Figure 42. Contours of Constant Speed for Multiple Jets

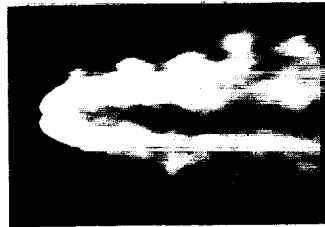
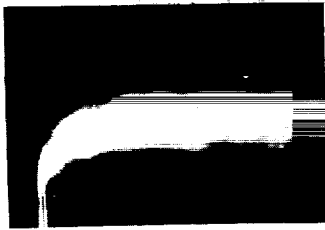


S/D = 4

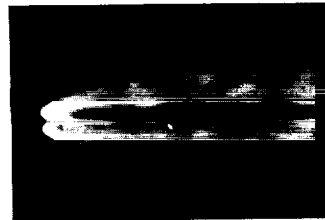
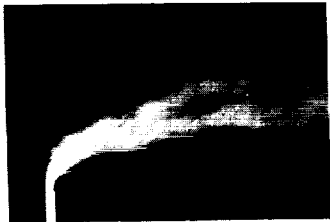


SIDE VIEW

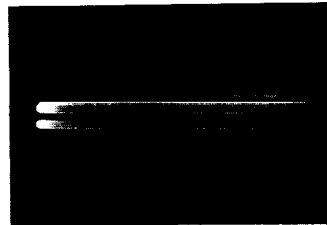
TOP VIEW



J = 70

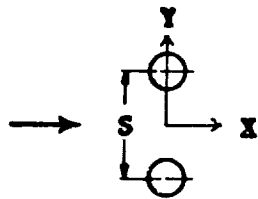


J = 40



J = 10

Figure 43. Smoke Photographs of Multiple Jets



$J = 18, S/D = 2$

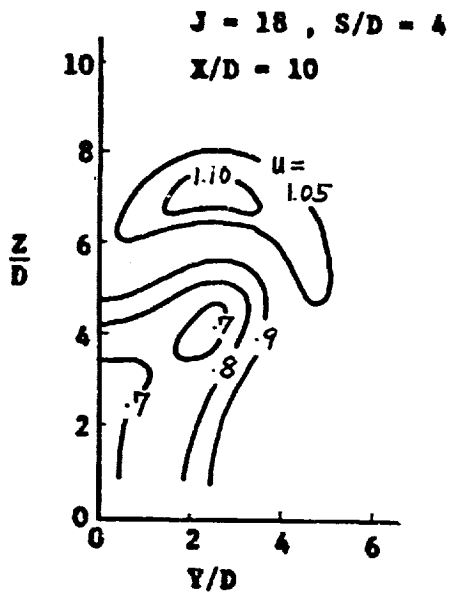
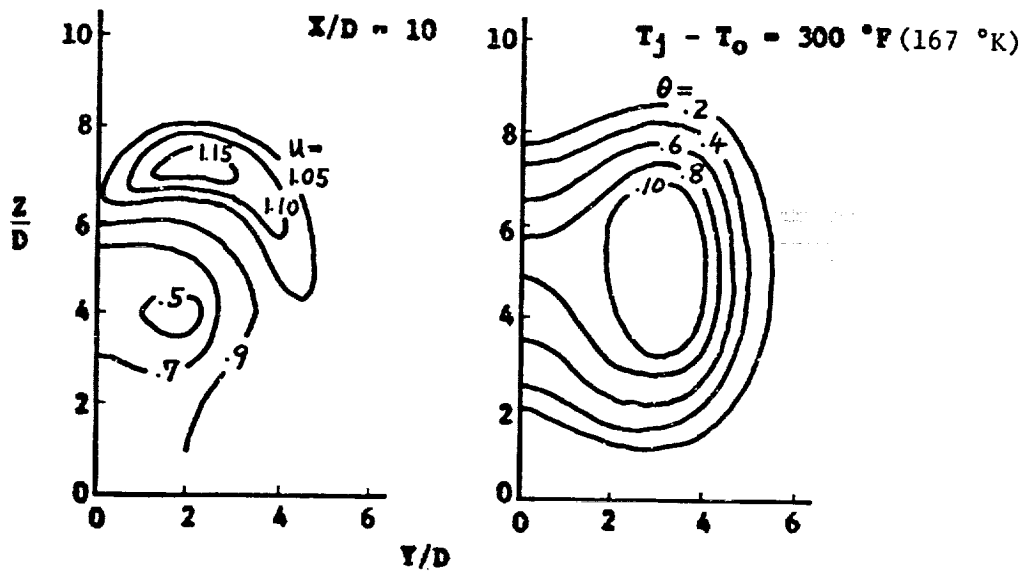


Figure 44. Contours of Constant Speed and Temperature for Multiple Jets

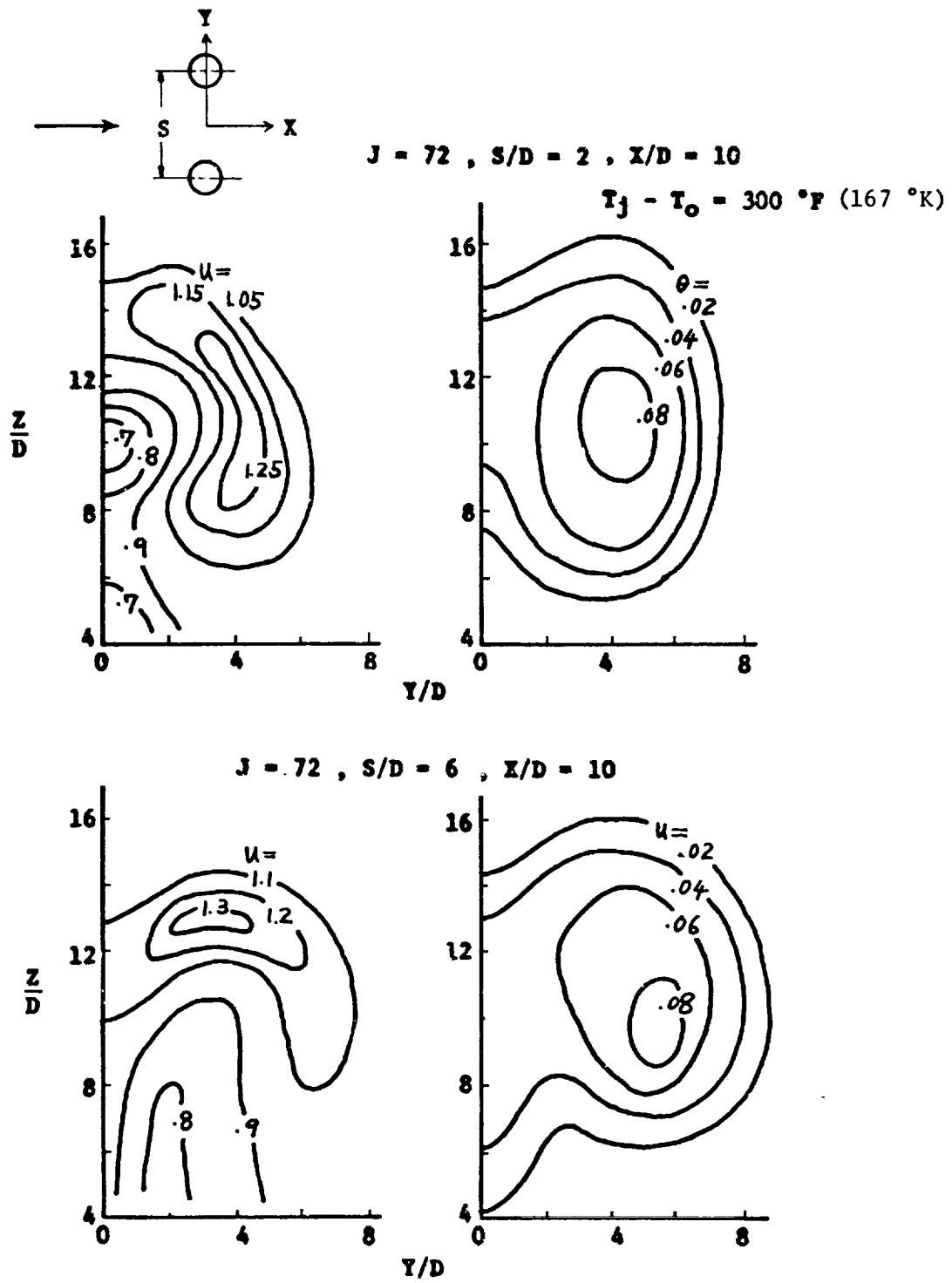
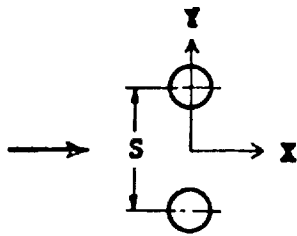


Figure 45. Contours of Constant Speed and Temperature for Multiple Jets



$J = 72, S/D = 4$

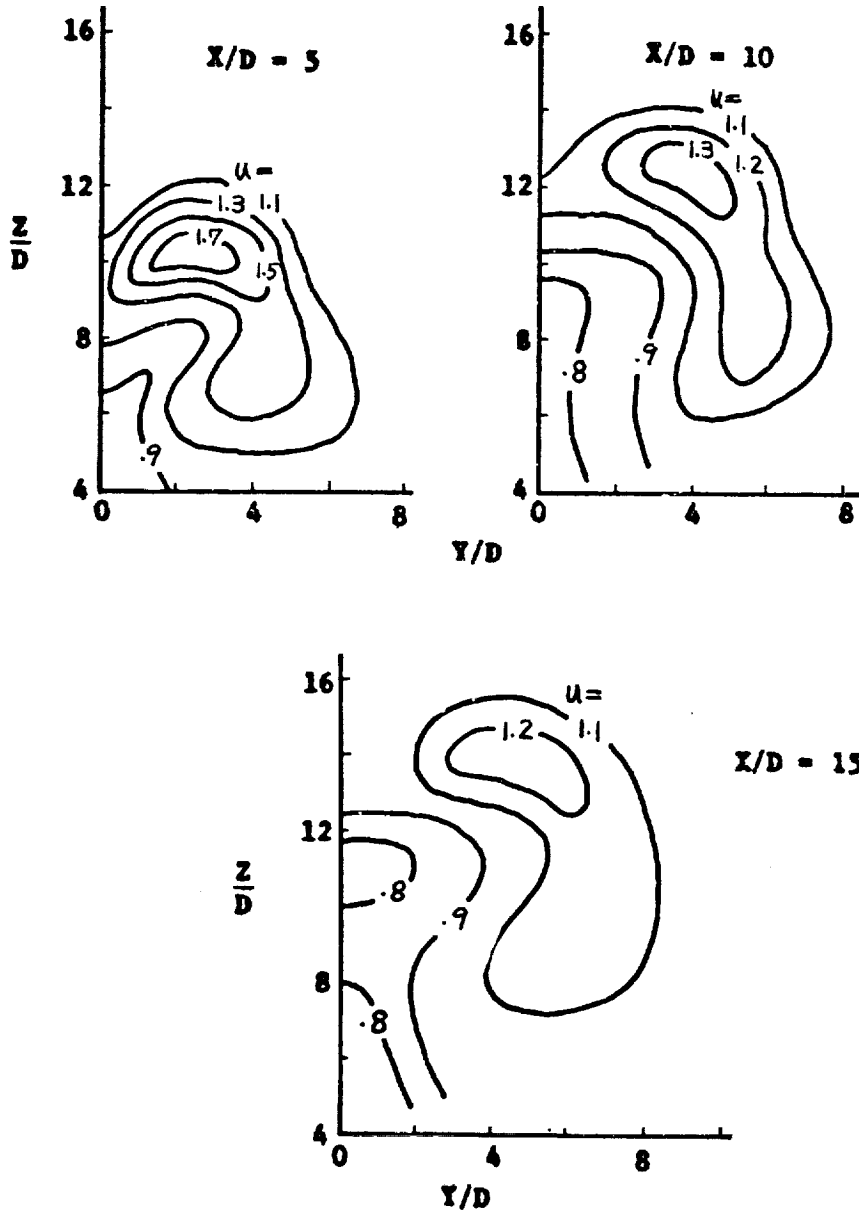


Figure 46. Contours of Constant Speed at Several Downstream Locations

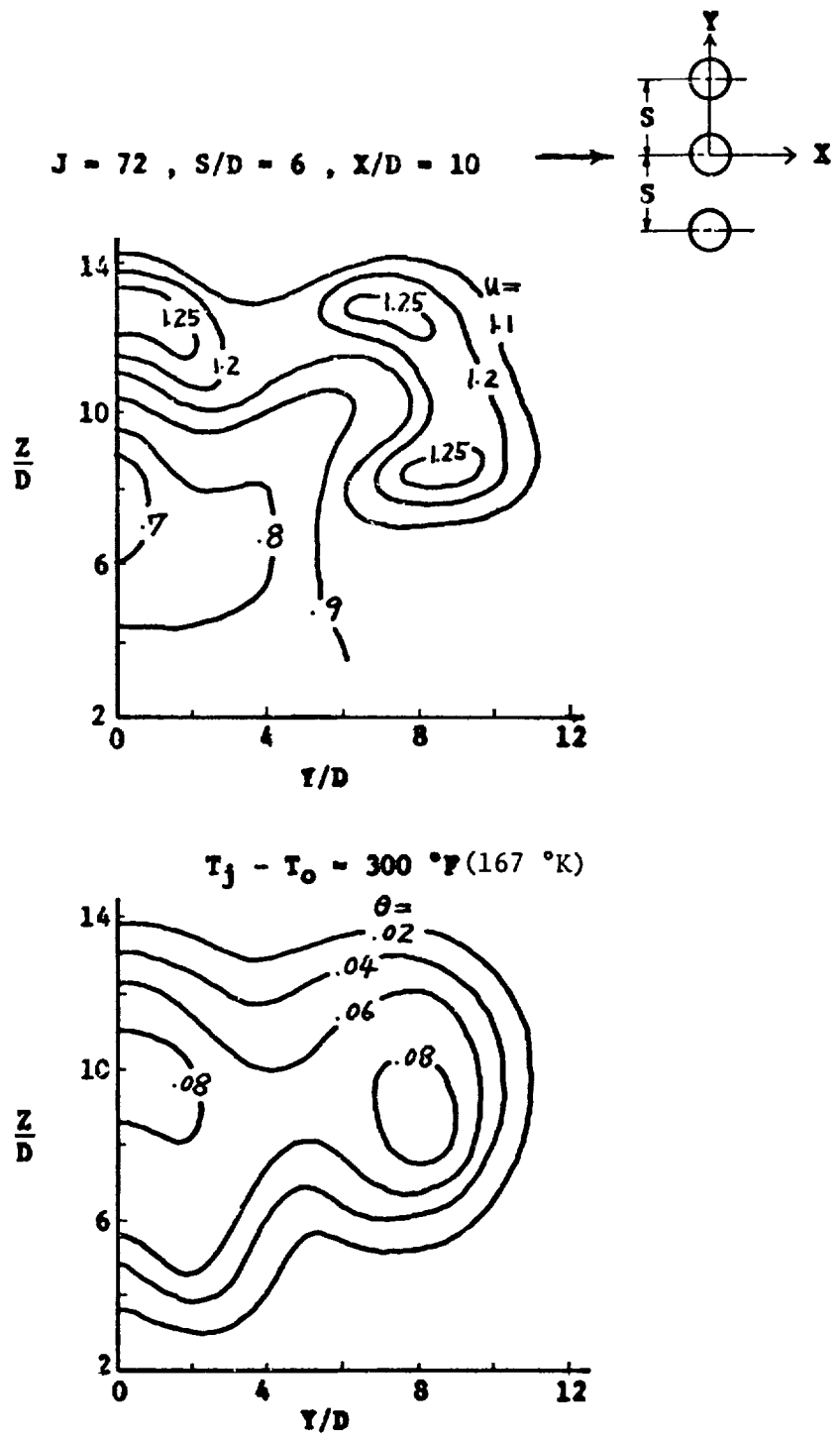


Figure 47. Contours of Constant Speed and Temperature for Multiple Jets

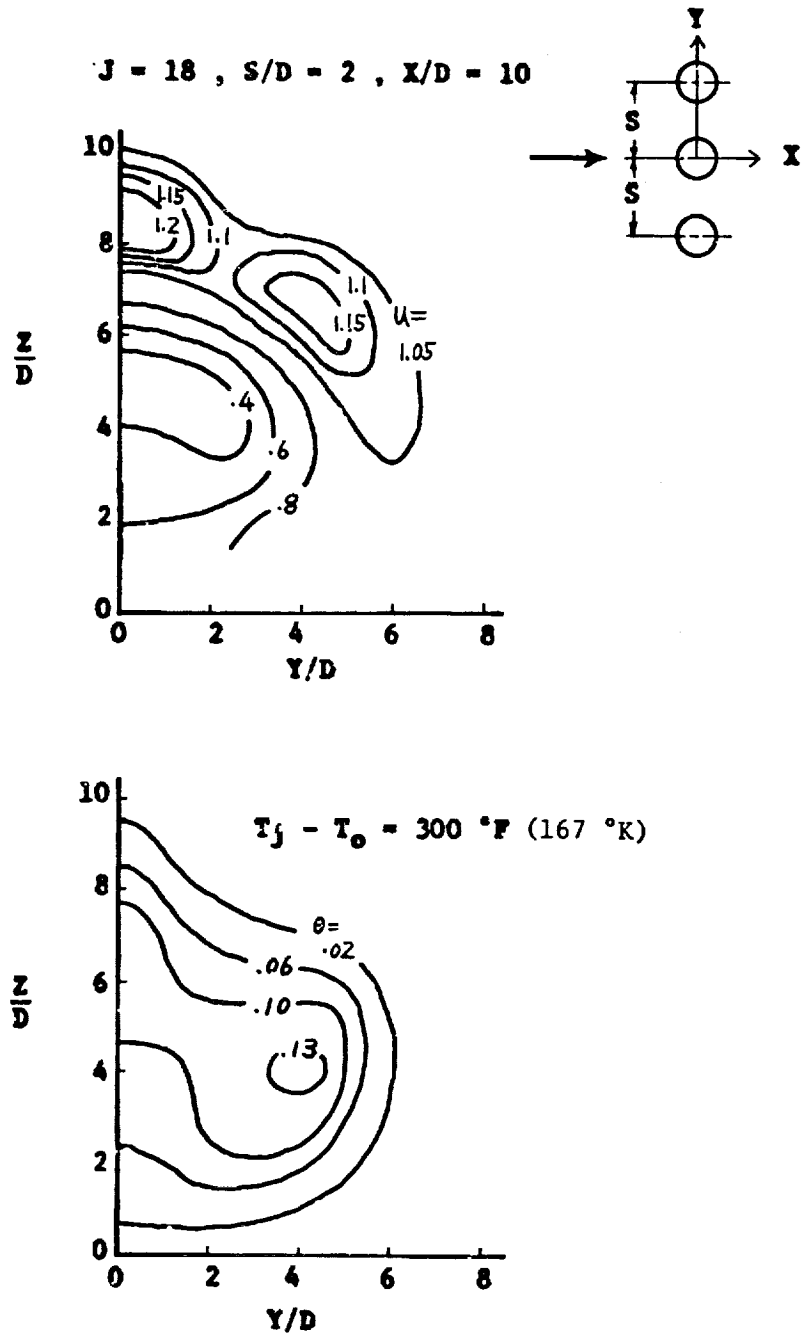
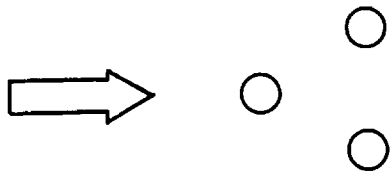


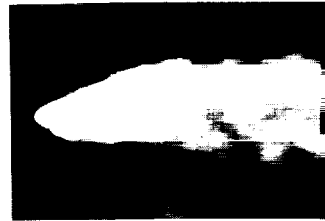
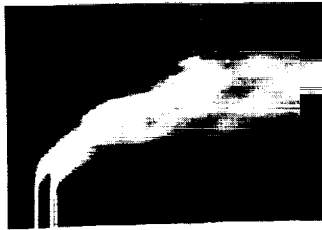
Figure 48. Contours of Constant Speed and Temperature for Multiple Jets



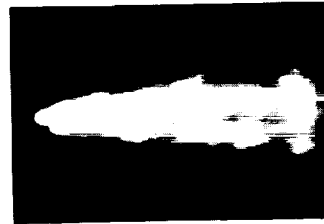
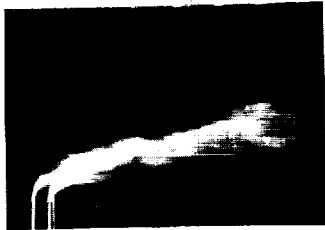
S/D = 4

SIDE VIEW

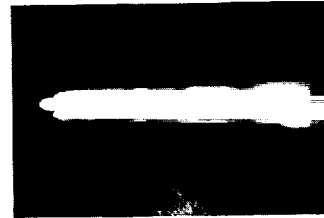
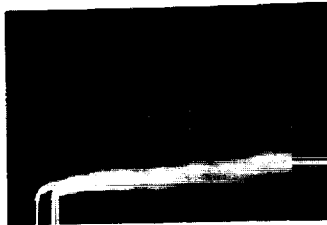
TOP VIEW



J = 70



J = 40



J = 10

Figure 49. Smoke Photographs of Multiple Jets

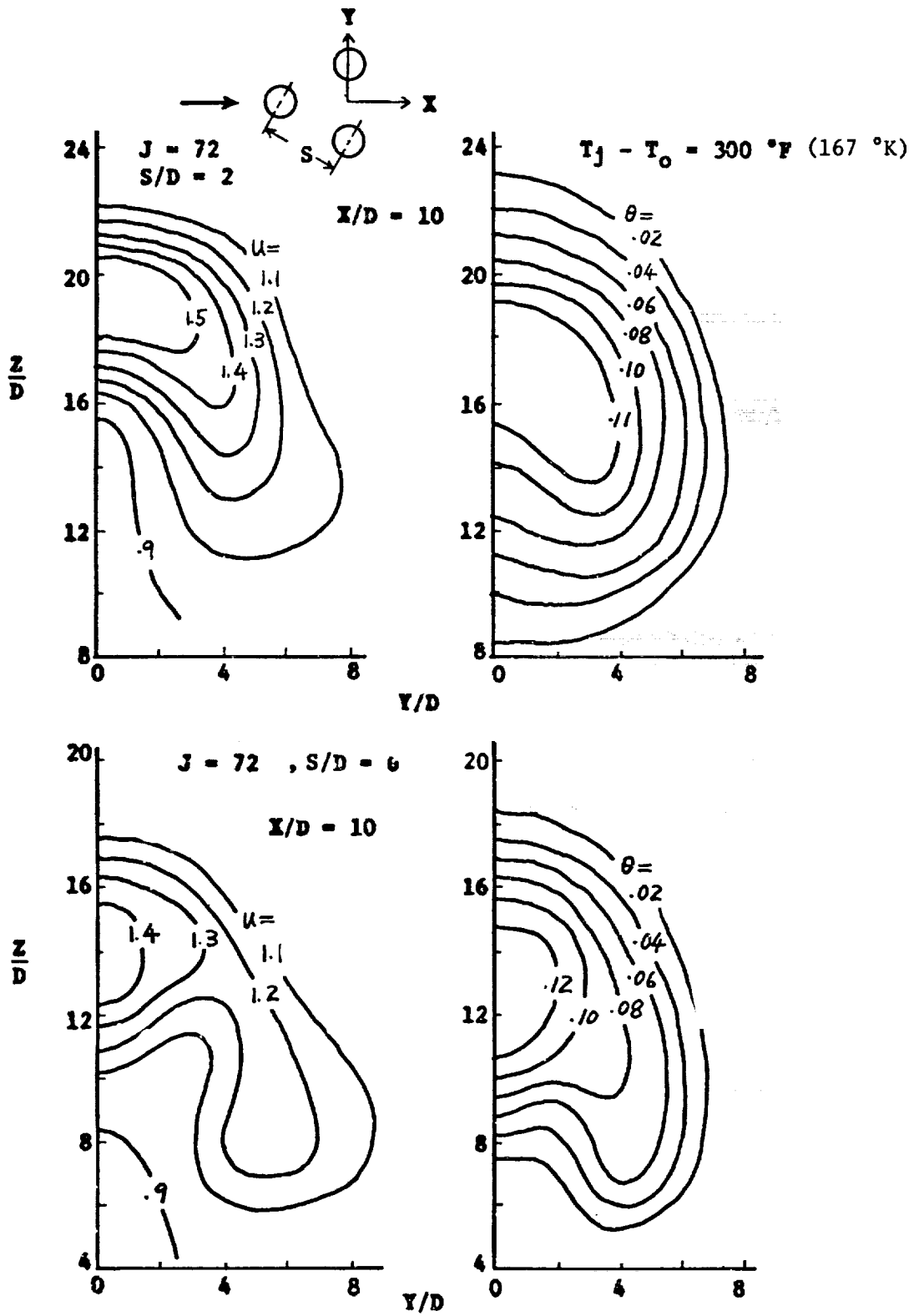
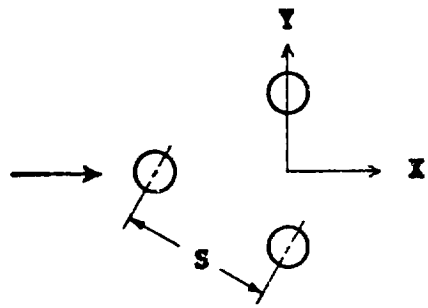


Figure 50. Contours of Constant Speed and Temperature for Multiple Jets



$J = 18$  ,  $S/D = 2$  ,  $X/D = 10$

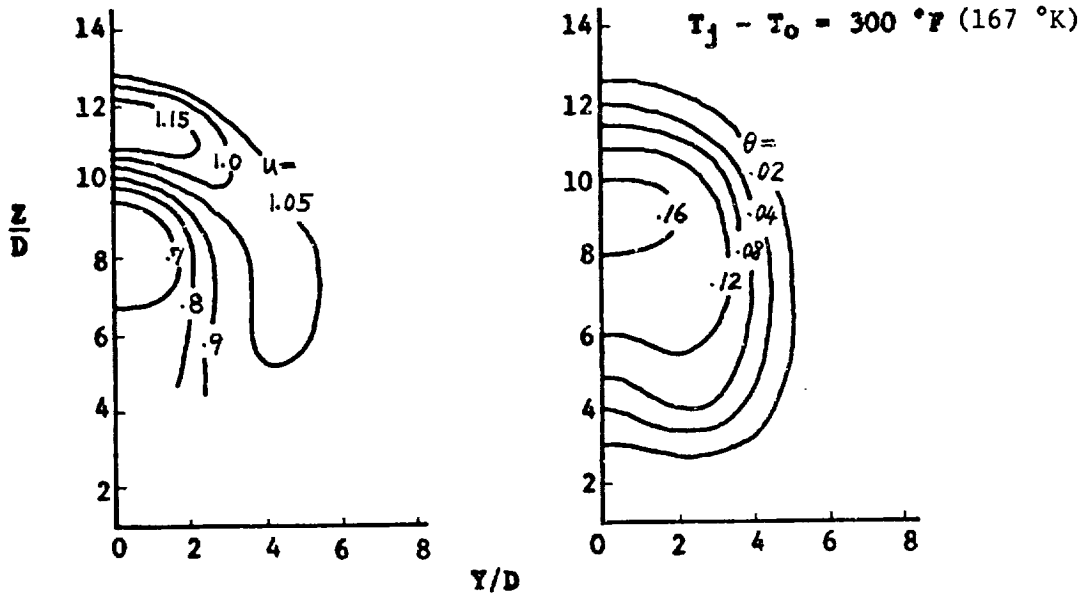
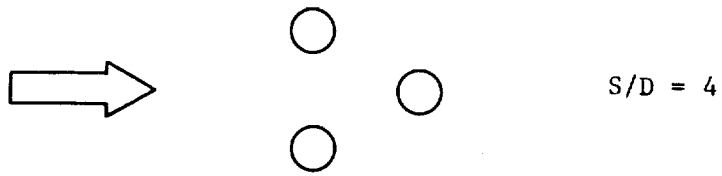
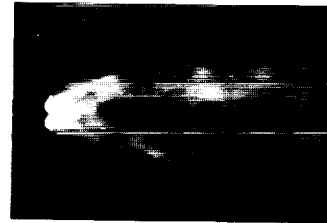
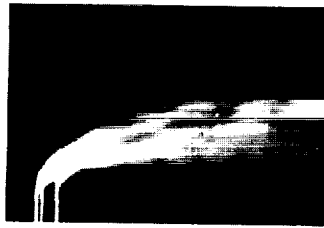


Figure 51. Contours of Constant Speed and Temperature for Multiple Jets



SIDE VIEW

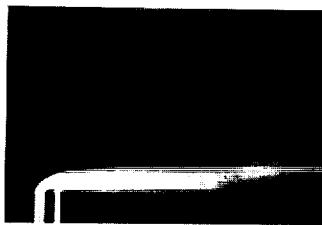
TOP VIEW



J = 70



J = 40



J = 10

Figure 52. Smoke Photographs of Multiple Jets

$J = 72$  ,  $S/D = 6$   
 $X/D = 10$

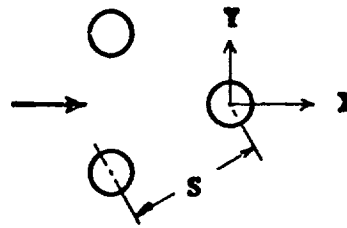
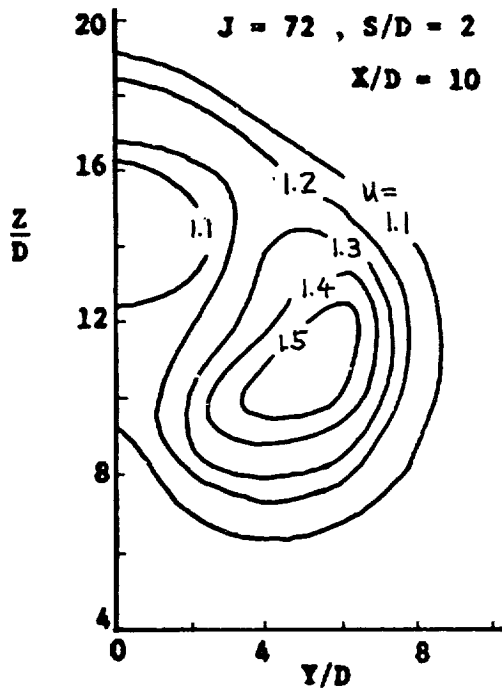
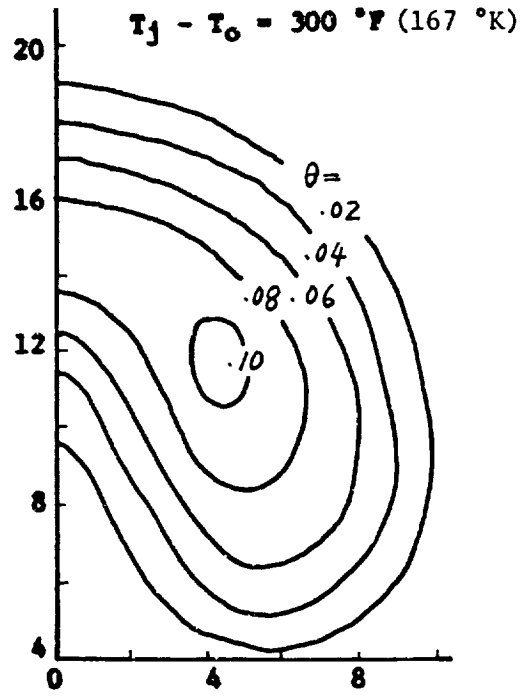
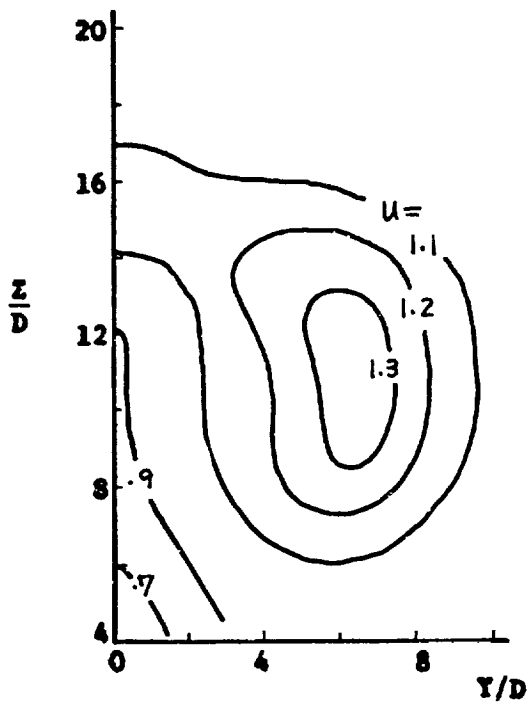


Figure 53. Contours of Constant Speed and Temperature for Multiple Jets

